

FINAL REPORT

A HIGH-PERFORMANCE ELECTROSTATIC
DISCHARGER FOR HELICOPTERS

A GOVERNMENT RESEARCH REPORT

U.S. DEPARTMENT OF COMMERCE

OFFICE OF TECHNICAL SERVICES

distributes this and thousands of similar reports in the interest of science, industry, and the public—for which research and new products mean better health, better living, and a stronger economy.

HOW TO GET OTHER REPORTS

The Office of Technical Services is the Nation's clearinghouse for reports of research supported by the Army, Navy, Air Force, Atomic Energy Commission, and other Government agencies.

Abstracts of new reports available are published twice a month in U. S. GOVERNMENT RESEARCH REPORTS (\$15 a year domestic).

Selected Reports of particular interest to small business are described monthly in TECHNICAL REPORTS NEWSLETTER (\$1 a year domestic).

Translations of foreign technical material are also available from the Office of Technical Services and other sources. These are listed or abstracted semimonthly in TECHNICAL TRANSLATIONS (\$12 a year domestic).

The above periodicals may be ordered from Superintendent of Documents, U. S. Government Printing Office, Washington, D. C., 20402, or through a U. S. Department of Commerce Field Office.

Inquiries about the availability of reports and translations on any particular subject may be directed to Office of Technical Services, U. S. Department of Commerce, Washington, D.C., 20230, or to any Commerce field office.

Reports and translations are published by the Office of Technical Services for use by the public. Thus, you may use the know-how or reprint the information therein except that where patent questions appear to be involved the usual preliminary search is advised, and where copyrighted material is used permission should be obtained for its further publication.

These documents are reprinted by OTS from the best available copy.

Task 1D121401A14130
(Formerly 9R38-01-017-30)

Contract DA 44-177-AMC-3(T)

TRECOM Technical Report 63-43

DECEMBER 1963

A HIGH-PERFORMANCE ELECTROSTATIC
DISCHARGER FOR HELICOPTERS

FINAL REPORT

REPORT NO. DCR-113

Prepared by:

DYNASCIENCES CORPORATION

for

U. S. Army Transportation Research Command
Fort Eustis, Virginia

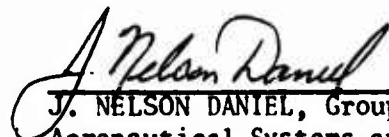
HEADQUARTERS
U S ARMY TRANSPORTATION RESEARCH COMMAND
FORT EUSTIS, VIRGINIA 23604

The work described in this report was performed by Dynasciences Corporation for the U. S. Army Transportation Research Command.

This Command concurs in the recommendations of the contractor.

Based on the work described herein, a development program for a higher capacity discharger for the CH-47 has been initiated.


S. BLAIR POTEATE, Jr.
Project Engineer


J. NELSON DANIEL, Group Leader
Aeronautical Systems and
Equipment Group

APPROVED.

FOR THE COMMANDER:

 2/c1
LARRY M. HEWIN
Technical Director

PREFACE

DYNASCIENCES CORPORATION, with the sponsorship of the U. S. Army Transportation Research Command (USATRECOM), Fort Eustis, Virginia, has designed, constructed, and flight tested a high-performance electrostatic discharging system for helicopters. Mr. Juan de la Cierva was the DYNASCIENCES project engineer and Mr. S. Blair Poteate was the cognizant USATRECOM project engineer.

This program was conducted from December 1962 to June 1963.

This report was prepared by J. de la Cierva, L. Egea, D. B. Fraser, and Dr. A. A. Perlmutter, and reviewed and approved by Dr. L. Goland.

The cooperation of the following organizations is gratefully acknowledged:

U. S. Army Aviation Test Board, Fort Rucker, Alabama.

U. S. Army Signal Corps Research and Development Laboratory, Milwaukee, Wisconsin.

U. S. Army Arctic Test Board, Fort Greely, Alaska.

U. S. Army Aviation Test Office, Edwards Air Force Base, California.

U. S. Marine Corps, Marine Air Group 36, Santa Ana, California

TABLE OF CONTENTS

	<u>Page</u>
PREFACE	iii
LIST OF ILLUSTRATIONS	vii
LIST OF TABLES	x
LIST OF SYMBOLS	xii
SUMMARY	1
CONCLUSIONS	2
RECOMMENDATIONS	3
TECHNICAL DISCUSSION	4
A. INTRODUCTION	4
B. STATEMENT OF THE PROBLEM	7
C. DISCHARGING DEVICE DESIGN CRITERIA	8
1. Helicopter Transfer Function	9
2. Sensing Unit Transfer Function	11
3. Control Unit Transfer Function	14
4. Power Amplifiers Transfer Function	20
5. High-Voltage Generators Transfer Function	20
6. Corona Point Probes Transfer Function	24
7. Discharging System Analysis	26
D. INSTRUMENTATION DESCRIPTION	43
E. EXPERIMENTAL PROCEDURE AND RESULTS	48
1. Engine-Exhaust-Mounted Corona Point Performance	48
2. Type 1 Discharger Performance	59
3. Type 2 Discharger Performance	60
4. Discharging System Radio Interference Measurements	70

	<u>Page</u>
F. ANALYSIS OF EXPERIMENTAL RESULTS	73
1. Discharging System Performance	73
2. Correlation of Theory and Experimental Data	75
3. Natural Charging Currents	76
4. Radio Frequency Interference	78
BIBLIOGRAPHY	79
APPENDIX A - ANALOGUE COMPUTER ANALYSIS	81
APPENDIX B - U. S. ARMY ELECTRONICS R & D LABORATORY LETTER SFIRA/FS	84
DISTRIBUTION	87

LIST OF ILLUSTRATIONS CONTINUED

<u>Figure</u>	<u>Title</u>	<u>Page</u>
17	Electrostatic Discharger Analogue Computer Set Up	37
18	V_H as a Function of Time, t , for Various Values of T_g (Computer Traces)	38
19	Type 2 Electrostatic Discharger Functional Block Diagram	40
20	V_H as a Function of Time, t , for Various Values of K_C (Computer Traces)	42
21	Instrumentation Test Bench, Configurations A and B	44
22	Instrumentation Bench Schematic Wiring Diagram	45
23	Time-Sync Unit	49
24	Exhaust Probe Installation on CH-37 Aircraft	51
25	Exhaust Probe Installation on CH-47A Aircraft	51
26	Current Polarity Convention	52
27	Engine-Exhaust-Mounted Corona Point Performance, CH-37 Aircraft	56
28	Engine-Exhaust-Mounted Corona Point Performance, CH-47A Aircraft	57
29	Probe Mount Loss Test Set Up	58
30	Type 1 System Transient Response, Gain 1	61
31	Type 1 System Transient Response, Gain 2	62
32	Type 1 System Transient Response, Gain 3	62
33	Type 1 System Transient Response, Gain 4	63

LIST OF ILLUSTRATIONS

<u>Figure</u>	<u>Title</u>	<u>Page</u>
1	Helicopter Electrostatic Discharger Block Diagram	10
2	Sensing Unit Schematic Diagram	12
3	Sensing Unit Installed on Test Aircraft Panel	13
4	Type 1 Control Unit Block Diagram	15
5	Type 1 Control Unit Schematic Diagram	16
6	Type 2 Control Unit Block Diagram	17
7	Type 2 Control Unit Schematic Diagram	18
8	Type 1 and Type 2 Control Units	21
9	Positive HVG Schematic Diagram	22
10	Negative HVG Schematic Diagram	23
11	High-Voltage Generators Installed in the Tail of Test Aircraft	25
12	Corona Point Probes, View from Aircraft Rotor Hub	25
13	Corona Point Probes Installed on Test Aircraft (Side View)	27
14	Corona Probe Installation Wiring Diagram	28
15	Type 1 Electrostatic Discharger Functional Block Diagram	30
16	Natural Frequency (ω_1) and Damping Ratio (γ) of the Discharging System as a Function of the High-Voltage Generator Time Constant (T_g)	35

LIST OF ILLUSTRATIONS CONTINUED

<u>Figure</u>	<u>Title</u>	<u>Page</u>
34	Type 1 System Transient Response, Gain 5	63
35	Type 1 System Performance in Cross-Country Flight Profile	64
36	Natural Charging Current Records (Fort Greely, Alaska)	66
37	Type 2 Discharging System Under Negative Saturation Conditions	66
38	Type 2 Discharging System Under Positive Saturation Conditions	67
39	Type 2 Discharging System Transient Response	67
40	Type 2 Discharging System High-Level Operation	68
41	Type 2 Discharging System High-Level Operation	68
42	Type 2 Discharging System in Arctic Cross-Country Flight Profile	69
43	Touch Tests, Fort Greely, Alaska	71
44	Radio Frequency Interference Measurements	71
45	Corona Point Probes Used in the RFI Measurements	74
46	Comparison of System Response to a Transient Without (Type 1) and with (Type 2) Dynamic Compensation	77

LIST OF TABLES

<u>Number</u>	<u>Title</u>	<u>Page</u>
1	Natural Frequency (ω_1) and Damping Ratio (ζ) of the Discharging System as a Function of the High-Voltage Generator Time Constant (T_g)	34
2	Recording Channel Assignments	47
3	Engine-Exhaust-Mounted Corona Point Performance Data, CH-37 Aircraft (Mojave)	54
4	Engine-Exhaust-Mounted Corona Point Performance Data, CH-47A Aircraft (Chinook)	55
5	UH-1 Helicopter Natural Charging Current Data, Arctic Environment	72

LIST OF SYMBOLS

C_H	= aircraft capacitance at a specific altitude
E_H	= electrostatic field intensity of aircraft at a given point
$F_{c,1}$	= transfer function of Type 1 electrostatic discharger system relating output I_d to input I_n ; a closed loop parameter
$F_{o,1}$	= transfer function in Type 1 electrostatic discharger system relating output I_d to input I_t ; an open loop parameter
I_{cp}	= total current flowing through the corona points
I_d	= current discharging the aircraft through corona break down of the air controlled by the electrostatic discharger system
$I_{d,ss}$	= steady state value of current discharged from aircraft through the corona point; equal to charging current by virtue of system operation
I_g	= current flowing through the ground drop line
I_n	= time rate of charge acquisition by the aircraft due to natural atmospheric conditions
I_R	= the portion of the corona current, I_{cp} , which recirculates to the aircraft
I_t	= net current charging the aircraft; the difference between I_n and I_d
K	= overall system steady state gain; the ratio of steady state system output V_H to system input I_n
K_1	= amplitude of step input
K_a	= transfer function of power amplifier relating output V_a to input V_c

K_{c1}	=	Transfer function of control unit of the Type 1 electrostatic discharger system
K_{c2}	=	multiplying factor of transfer function of the Type 2 electrostatic discharger system; consists of two factors one being K_{c1} , the other determined by the compensator components
K_{cp}	=	transfer function of corona point relating output corona current to input corona point voltage
K_g	=	steady state gain of high-voltage generator
K_s	=	transfer function of sensor relating output voltage V_s to input V_H
ω_1	=	natural radian frequency of oscillatory transient component of system response V_H to a step input I_n
ψ	=	phase angle of oscillatory transient component of system response V_H to a step input I_n
s	=	Laplacian operator
T_c	=	time constant of corona point high-voltage supply effectively replacing T_g through operation of the compensator unit
T_g	=	time constant of corona point high-voltage supply
T_1	=	defined by Equation 24
t	=	time, seconds
V_a	=	output voltage of power amplifier; input to high-voltage generator
V_c	=	output voltage of control unit; input to power amplifier
V_{cp}	=	D.C. high-voltage applied to corona point which causes corona to occur; output of high-voltage generator

- V_H = potential the aircraft assumes relative to earth caused by the net charging current I_t
- $V_{H,ss}$ = steady state value of aircraft potential produced by electrostatic discharger system operation
- V_s = output voltage of sensor; input to control unit
- ζ = damping ratio of oscillatory transient component of system response V_H to a step input I_n

SUMMARY

↙ This report contains the results of a program concerned with the design, construction, and flight testing of a high-performance static electricity discharging system for helicopters. Flight test data showed that the discharging system kept the electrostatic energy of a CH-37 helicopter below 1 millijoule for natural charging currents of up to 50 microamperes. This is in accordance with the established design specifications. Data were also obtained on the radio interference characteristics of the system and on the performance of corona points located in the engine exhaust stream.

CONCLUSIONS

The following conclusions can be drawn as a result of the work performed in this program:

- a. The discharging system meets the design specifications of keeping the electrostatic energy of a CH-37 helicopter below 1 millijoule (1,200 volts at 5 feet of altitude) for natural charging currents of up to 50 microamperes.
- b. The system concept used in this program can be adapted to meet any other discharging requirements.
- c. The performance of corona points located in the engine exhaust stream is approximately symmetric with respect to polarity, and the corona point currents correspond to those obtained in a previous test program (Reference 2).
- d. The discharging system, with the exception of the corona points, satisfies the radio interference specifications of MIL-I-11748B. The radio interference characteristics of the corona points need further evaluation before definite conclusions can be made.
- e. Discharger characteristics required for the various helicopters should be determined during actual operations.

RECOMMENDATIONS

The following recommendations are made:

- a. A systematic survey of the charging characteristics of helicopters operating under various climatic and atmospheric conditions should be conducted. This survey should be performed by installing Type 2 electrostatic dischargers, as described on page 14, and slow-speed recorders in a number of operational helicopters.
- b. Investigations of the radio interference characteristics of corona points and of techniques for suppressing such interference should be continued.

TECHNICAL DISCUSSION

A. INTRODUCTION

The research program, which constitutes the subject of this report, included phases of study, design and construction of instrumentation and test equipment, and testing. For the sake of clarity, a brief chronological description of these phases is presented in this introduction. The phase numbers and descriptions in this chronology will be utilized throughout this report to identify and correlate the procedures and findings of this program.

It is noted that two types of discharge systems are reported in this report and are identified as Type One and Type Two Discharging Systems. After the analysis of the data taken during the flight testing of the Type One System, it was decided that a modification to the control circuitry was necessary to provide the proper system dynamics. The addition of the dynamic compensating network to the control unit circuitry was made. The discharging system incorporating this modification is known as the Type Two Discharging System. The Type One and Type Two Systems are the same in all respects with the exception of the control unit.

The chronology of the program was as follows:

<u>Phase No.</u>	<u>Period</u>	<u>Location</u>	<u>Description</u>
1	Dec. 62 to Jan. 63	Contractor's Plant	<u>Study</u> : System dynamic analysis. <u>Design Criteria</u> : Computer studies. Instrumentation requirements.
2	Jan. 63	Contractor's Plant	<u>Design</u> : Discharging system electronic and mechanical design. Instrumentation design.
3	Jan. 63	Contractor's Plant	<u>Construction</u> : Discharging system construction (Type 1) Instrumentation Construction.
4	Jan. 63	Contractor's Plant	<u>Bench Testing</u> : Discharging system dynamic testing. Instrumentation testing.

<u>Phase No.</u>	<u>Period</u>	<u>Location</u>	<u>Description</u>
5	Jan. 63	Contractor's Plant	<u>Radio Interference Bench Testing:</u> Conduction and radiation interference test of the discharging system, except the corona point probes. This phase was performed with the assistance of the U. S. Army Signal Corps R & D Lab., Field Station No. 1, Milwaukee, Wisconsin.
6	Jan. 63	Ft. Rucker, Alabama	<u>Engine Exhaust Corona Point Performance Measurements:</u> In-flight measurement of the performance of high-voltage corona point probes installed in the exhaust stream of reciprocating and gas turbine engines. This test was conducted in CH-37 and CH-47 aircraft.
7	Feb. 63	Ft. Rucker, Alabama	<u>Type 1 Discharging System In-Flight Checkout:</u> Determination in flight of the static and dynamic characteristics of the discharging system having a Type 1 control unit and installed in a CH-37 aircraft. Sensor sensitivity calibration.
8	Feb. 63	Contractor's Plant	<u>Discharging System Modification:</u> As a result of the data obtained in Phase 7, it was considered advisable to modify the system dynamics in order to improve its performance. This phase includes the design and construction work required to complete this modification. This resulted in the Type 2 discharging system.

<u>Phase No.</u>	<u>Period</u>	<u>Location</u>	<u>Description</u>
9	Mar. 63	Ft. Greely, Alaska	<u>Type 2 Discharging System Flight Testing:</u> Static and dynamic measurements of the performance of the Type 2 discharging system installed in a CH-37 aircraft. In addition, this phase included measurements of the natural charging currents under several flight conditions for CH-37, UH-1B, and UH-1D Army helicopters.
10	Mar. 63	Edwards AFB, California	<u>Corona Point Radio Frequency Interference Measurements:</u> Determination of the radio frequency interference characteristics of high- voltage designs, installed on a CH-37 helicopter. Results compared against MIL-I-11748B (Sig. C).

B. STATEMENT OF THE PROBLEM

It is a well-known fact that all aircraft flying in the atmosphere are subject to electrostatic charge build-ups. In recent years, the U. S. Army has conducted an extensive research effort to alleviate the problems arising from this phenomenon.

The mechanisms producing the electrostatic charging have been investigated in References 1 through 5, and several types of discharging devices are described in References 1, 2, 4, and 5.

The magnitude of the natural charging currents occurring in various types of helicopters under several environmental conditions has been reported recently in Reference 6. In addition, the levels of electrostatic energy acceptable for helicopter operations and the capacitance of several types of rotary-wing aircraft were determined and reported in References 1 and 2. The performance of a high-voltage corona point as a function of air speed for several corona point configurations was also determined in References 1 and 2.

The information obtained during these research programs, all of which were performed prior to the program discussed herein, led to the formulation of the desired characteristics for an electrostatic discharging system. These characteristics define the performance that is required to maintain the electrostatic energy of a helicopter below an acceptable level. The characteristics are as follows:

Maximum Acceptable Electrostatic Energy Level on a Helicopter	1 Millijoule
Maximum Expected Natural Charging Current in Heavy Helicopters (gross weight on the order of 33,000 lbs.)	\pm 50 Microamperes
Maximum Voltage Level Acceptable on the Helicopter (based on the above maximum energy level and the helicopter capacitance measurements, Reference 1, 5 foot altitude)	1.2 Kilovolts

Corona Point Probe Voltage, Required
To Discharge 50 Microamperes
(using a design consisting of two
points per polarity)

60 Kilovolts

In addition, company-sponsored research work performed at DYNASCIENCES CORPORATION showed that an important characteristic of a high-performance discharging system is its dynamic stability. This is illustrated by the fact that the rate of voltage build-up in a CH-37 helicopter under 50 microamperes charging current is as high as 66 kilovolts per second. Consequently, the time constant of all system components should be sufficiently small to allow a suitable system response before the aircraft voltage exceeds the established safe level. The importance of the dynamic characteristics of the discharging system has been confirmed by the experimental results reported herein, as will be shown in subsequent sections.

The primary purpose of the program discussed herein was to design, build, and flight test a high-performance electrostatic discharger for helicopters having characteristics in accordance with the discussion of the preceding paragraphs. Additional objectives of this research program were:

1. Measurement of the performance of high-voltage corona point probes installed in the engine exhaust gas stream of CH-37 Mojave and CH-47 Chinook Army helicopters.
2. Determination of the radio interference characteristics of the discharging system. This included conduction and radiation tests of the discharging equipment as well as of the corona probe by itself.

These objectives were successfully achieved during the program. In addition, new information was obtained on the magnitudes of natural charging currents affecting normal types of helicopters in arctic and desert climates; instrumentation techniques were developed and tested to study and analyze aircraft electrostatic charging phenomena.

C. DISCHARGING DEVICE DESIGN CRITERIA

An electrostatic discharging device can be considered as an

automatic control system which maintains the helicopter's external electrostatic field within prescribed values when under specified excitations. Figure 1 represents a block diagram of the discharging system and includes the symbol convention to be used hereinafter.

The natural charging current, I_n , can be considered as the system input (excitation) signal. The system discharging current, I_d , must equal the natural charging current under steady-state conditions if V_H is below the helicopter corona threshold. The magnitude and polarity of the system discharging current, I_d , are determined by the magnitude and polarity of the helicopter voltage, V_H , as measured by the sensing unit and processed by the remaining system components. Consequently, the overall closed loop system gain is determined by the specified characteristics of the discharger once the helicopter transfer function becomes known. The analysis of an automatic control system requires that the transfer function of all system components be known. This section describes the philosophies utilized in establishing the transfer function of each system component.

1. Helicopter Transfer Function

With the discharger in operation, the helicopter can be considered as a pure capacitor. This is due to the fact that with proper discharger operation, the helicopter electrostatic field is at a sufficiently low level that no corona discharge occurs at any point on the aircraft other than at the discharging system probes. By comparing the helicopter to a capacitor, the electrostatic behavior of the helicopter can be represented by the following transfer function:

$$\frac{E_H}{I_t} = \frac{1}{C_H s} \quad \frac{\text{VOLTS}}{\text{AMPERE-METER}} \quad (1)$$

where the notation corresponds to that on Figure 1, and s is the Laplace transform operator. Consequently, the gain of the helicopter transfer function is the inverse of the helicopter capacitance.

It should be noted, however, that the capacitance of the aircraft is not at a constant magnitude throughout

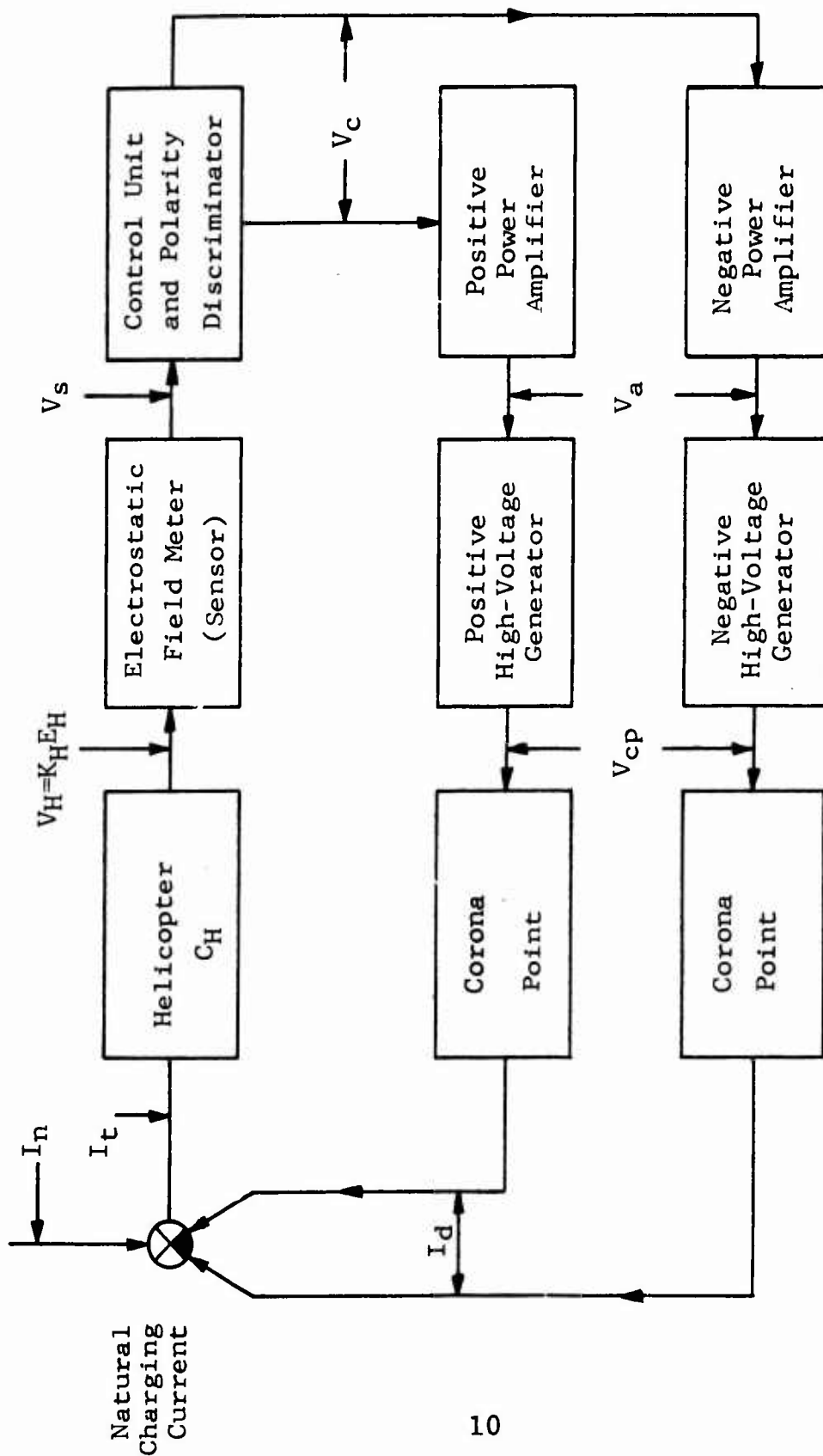


FIGURE 1: HELICOPTER ELECTROSTATIC DISCHARGER
BLOCK DIAGRAM

the flight envelope. In fact, during low-altitude hovering flights, when the proper functioning of the discharging system is essential, this capacitance varies rapidly with the aircraft altitude (Reference 1). This variation may be considered as an additional system input which cannot be differentiated from an I_n input by the system sensing element, because both inputs are measured by the system sensor as field changes.

In order to compensate for the changes in capacitance, the present system has been designed by assuming a constant aircraft capacitance equal to the largest value present in helicopter flight (10^{-9} farad). Therefore, a decrease in the aircraft capacitance due to higher flight altitudes is equivalent to an increased system overall gain, as shown by Equation (1).

2. Sensing Unit Transfer Function

The sensing unit used in the program described herein was a modification of a Government-furnished electrostatic field meter, which was built under U. S. Army Contract DA 44-177-TC-652. It consisted basically of a rotating-vane generating voltmeter, followed by a transistorized A-C amplifier and a synchronous polarity discriminator. This sensing unit, in its unmodified form, was not suitable for a high-performance discharging system, mainly because of its long time constant.

A temporary solution to improve the dynamic response of the sensor unit was effected by stepping up the driving motor speed by a factor of 5 and by eliminating the phase retarding capacitors in the amplifier. However, the increased motor speed was found to produce a substantial reduction of the life of the slip-ring assembly used for the synchronous demodulation. Figure 2 presents the schematic diagram of the sensing unit, and Figure 3 shows its installation in the test aircraft.

The time constant of the modified sensing unit was measured and found to be 8 milliseconds. This value

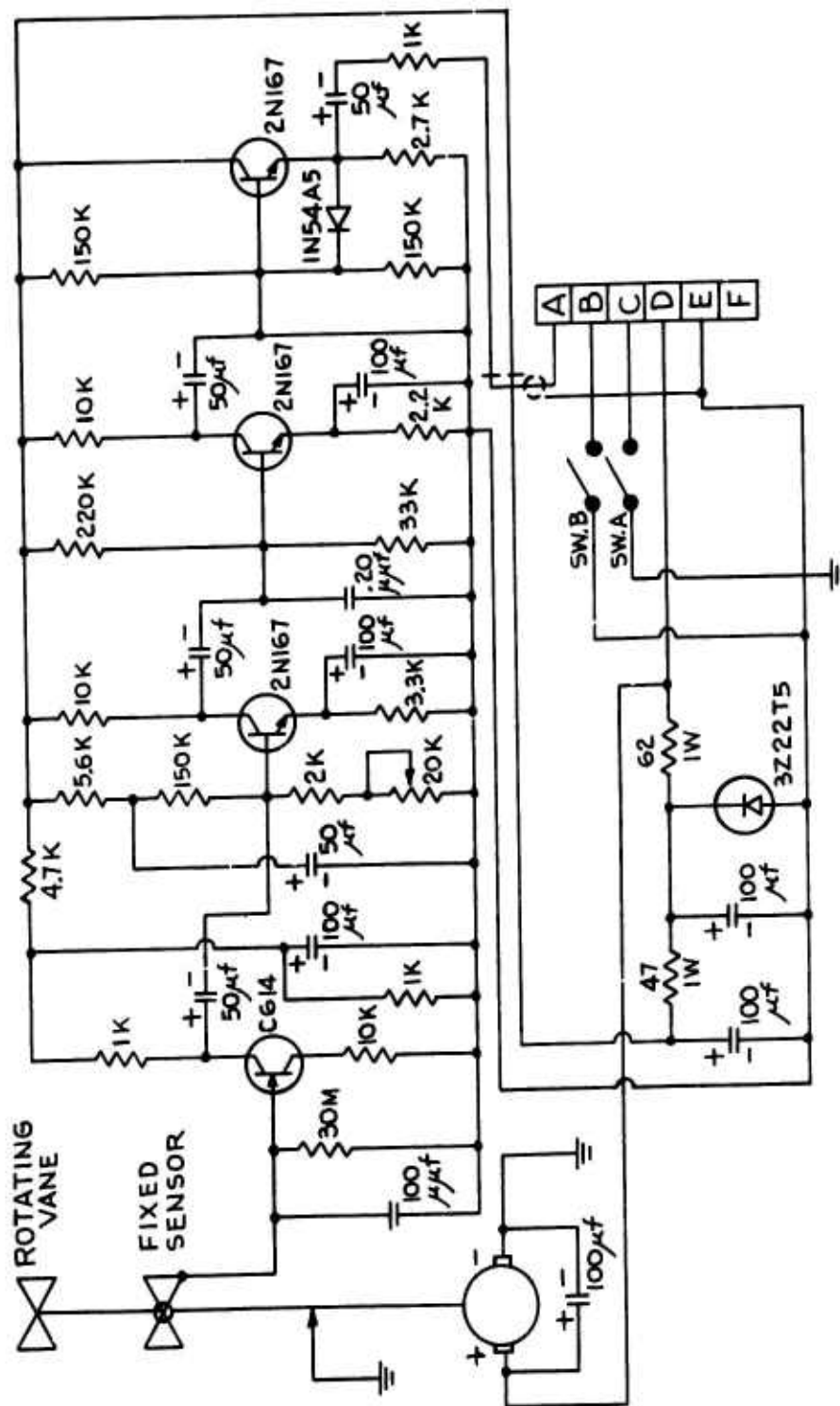


FIGURE 2: SENSING UNIT SCHEMATIC DIAGRAM

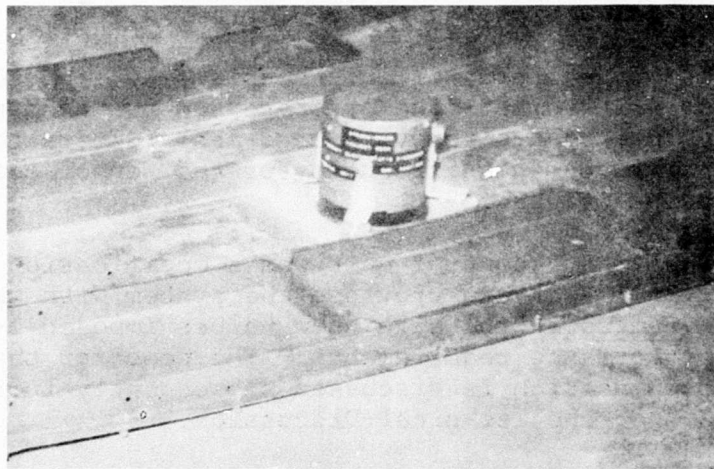
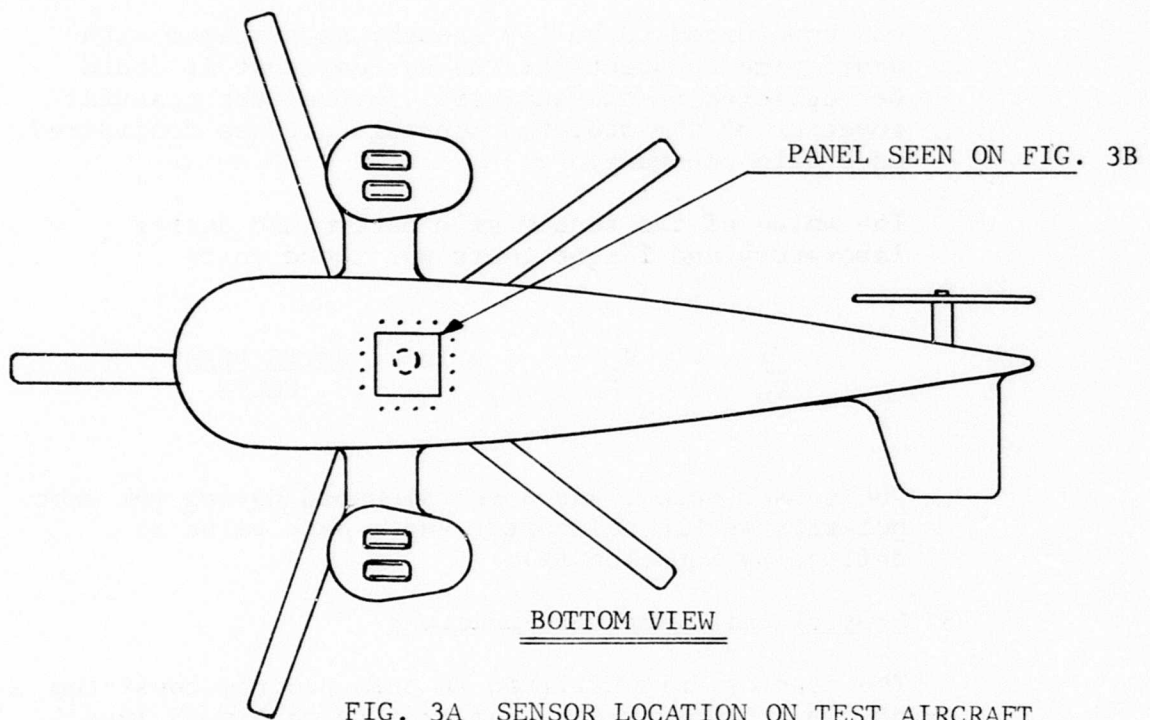


FIG. 3B

FIGURE 3: SENSING UNIT INSTALLED ON TEST AIRCRAFT PANEL

was considered to be low enough, as compared with other time constants of the system, that it could be neglected in the analysis. Hence, the transfer function of the modified sensing unit was considered as a gain constant.

The value of the sensor gain determined during laboratory and flight tests was found to be

$$\frac{V_s}{V_H} = K_s = 3 \times 10^{-3} \frac{\text{VOLTS PEAK}}{\text{VOLTS}} \quad (2)$$

The sensor output was a semisinusoid having the same polarity as the helicopter and a peak value as defined by Equation (2).

3. Control Unit Transfer Functions

The control unit utilized in this program consisted of two configurations, referred to herein as Type 1 and Type 2. Figure 4 is a block diagram of the Type 1 Control Unit, and Figure 5 presents the corresponding schematic diagram.

The Type 1 control unit consists of a diode-type polarity discriminator stage and two (one per polarity) D-C removing band-pass filters tuned to the fundamental frequency of the sensor semisinusoidal output signal.

The Type 2 control unit was a modification of the Type 1 unit and provided the system with the proper dynamics at the high gain values imposed by the performance requirements. The need for the dynamic compensation is discussed subsequently in Section C.7 of the Technical Discussion.

Figure 6 presents a block diagram of the Type 2 control unit. The corresponding schematic diagram is shown in Figure 7. The transfer functions of the control units were selected as

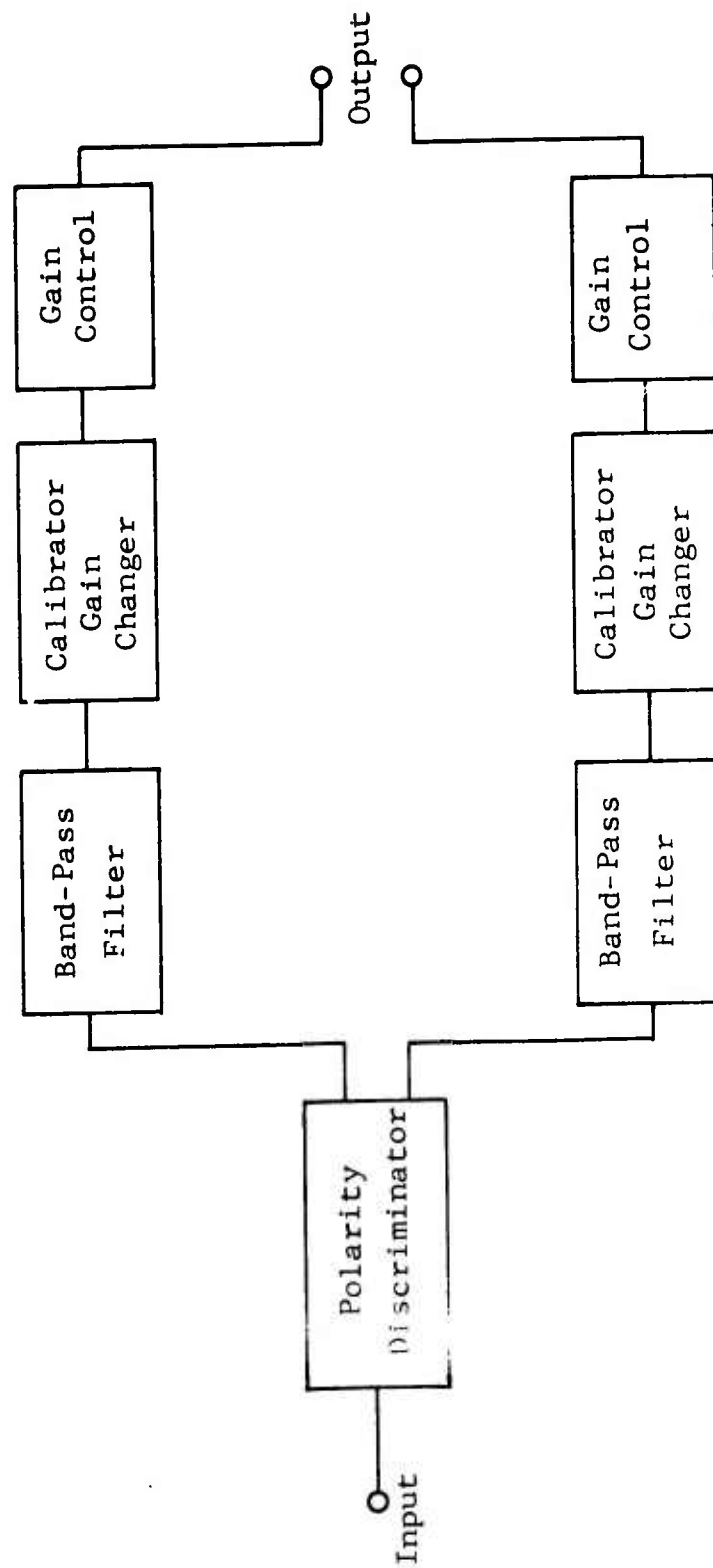


FIGURE 4: TYPE 1 CONTROL UNIT BLOCK DIAGRAM

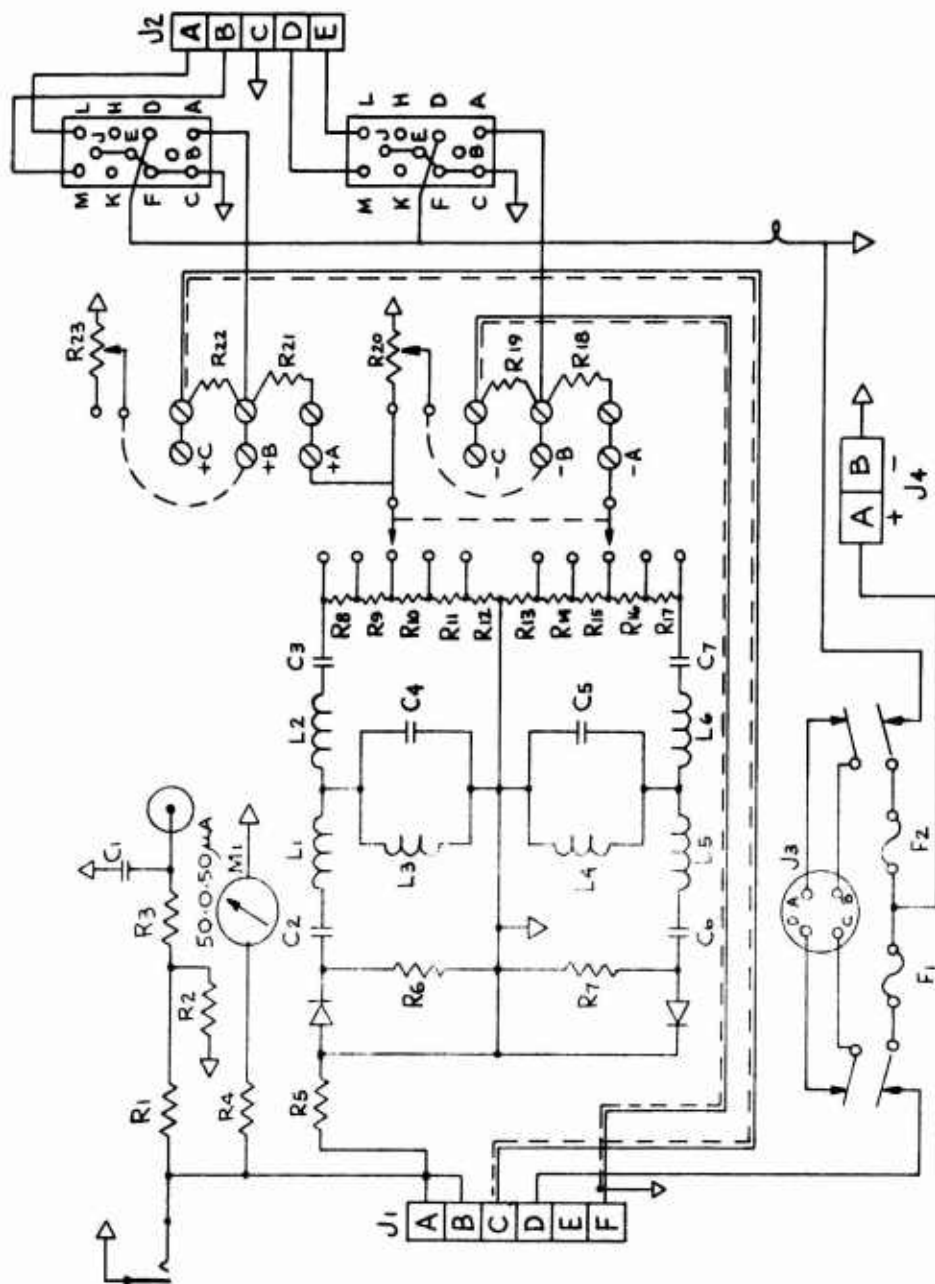


FIGURE 5: TYPE 1 CONTROL UNIT SCHEMATIC DIAGRAM

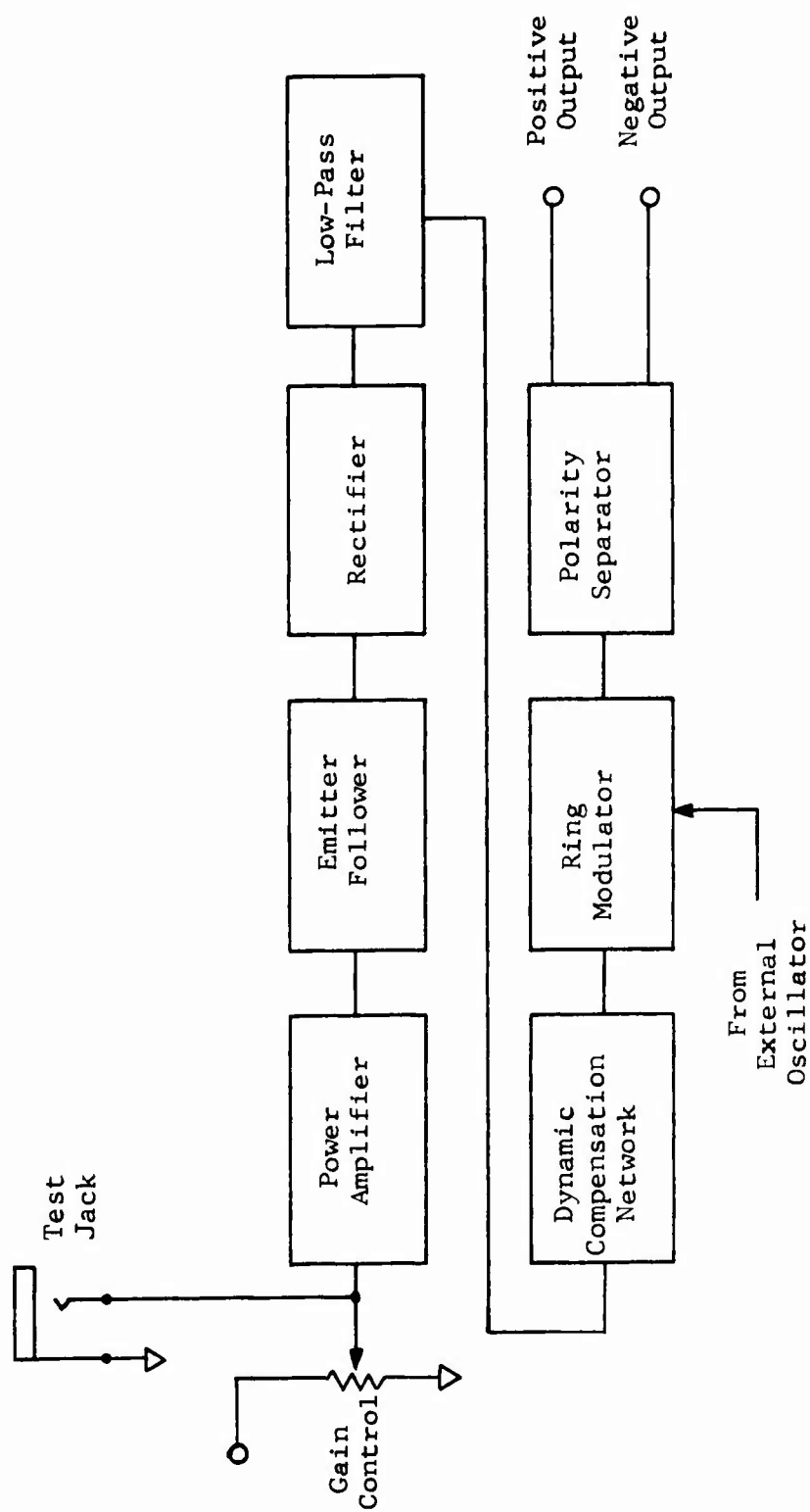


FIGURE 6: TYPE 2 CONTROL UNIT BLOCK DIAGRAM

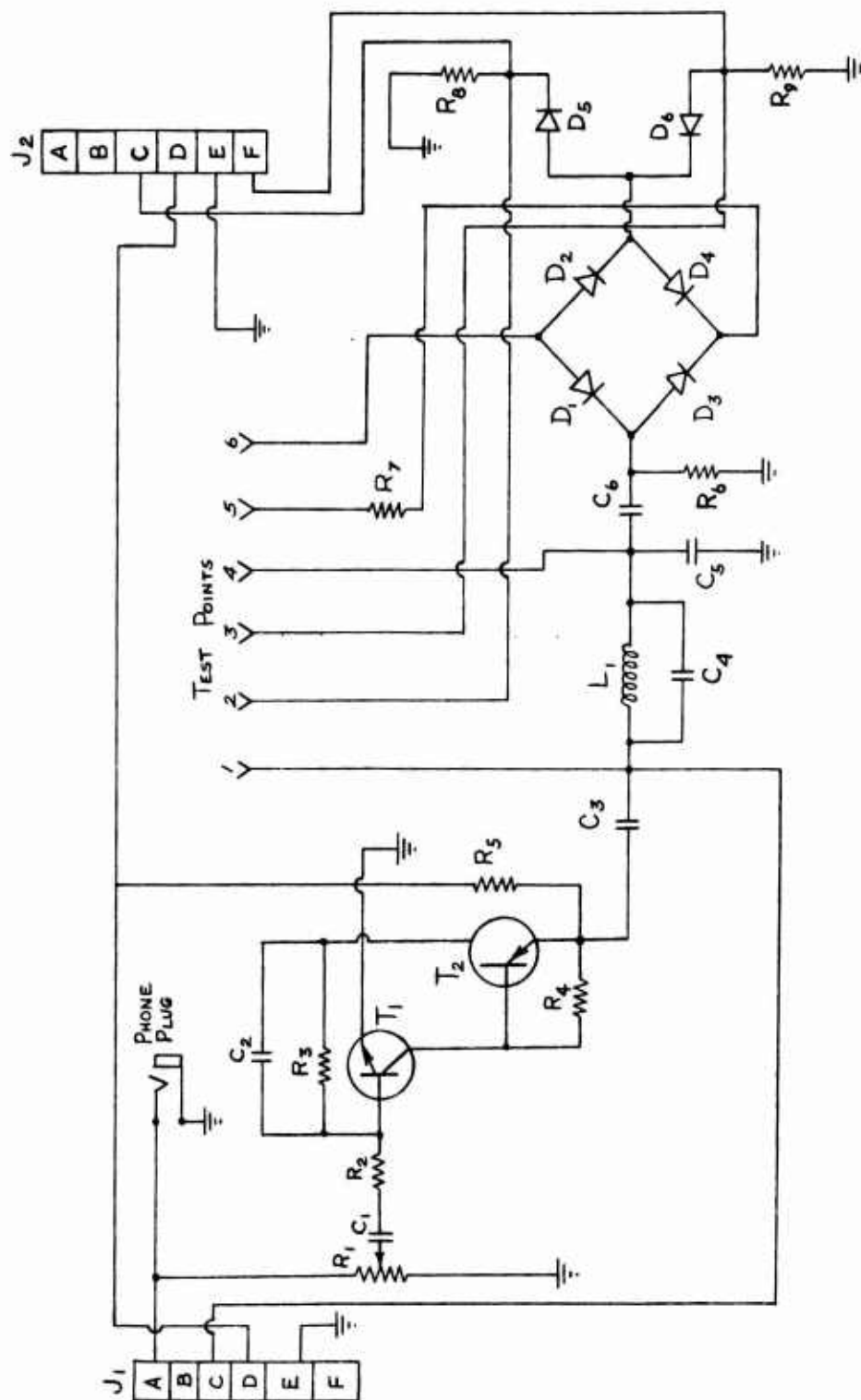


FIGURE 7: TYPE 2 CONTROL UNIT SCHEMATIC DIAGRAM

$$\text{Type 1: } \frac{V_c}{V_s} = K_{c1} \frac{\text{VOLTS PEAK}}{\text{VOLTS PEAK}}, \quad \text{and} \quad (3)$$

$$\text{Type 2: } \frac{V_c}{V_s} = K_{c2} \frac{(1+T_g s)}{(1+T_c s)} \frac{\text{VOLTS PEAK}}{\text{VOLTS PEAK}} \quad (4)$$

K_{c1} and K_{c2} were adjustable, and separate gain controls were provided to compensate for any polarity channel asymmetry. The values of K_{c1} and K_{c2} were varied during the flight testing to determine experimentally the effect of the system gain on its dynamics. The values of both K_{c1} and K_{c2} were

Gain Setting	1	2	3	4	5	
$K_{c1} \times 10^3$	2.67	5.34	8	10.7	13.31	(5)
$K_{c2} \times 10^3$			13.31			

The selection of the transfer functions of the control units as well as the value of their gain constants will be explained subsequently in Section C.4.

The values of T_g and T_c were chosen to provide optimum compensation of the system dynamics. Values of 0.300 second for T_g and 0.03 second for T_c were originally chosen. These values, as will be shown subsequently in this report, lead to a system damping ratio of 0.35; this is considered to be very satisfactory for the electrostatic discharging system under study.

D-C power switches for the sensor and high-voltage stages were also located on the control unit. In addition, a D-C signal proportional to the sensor output was provided for recording purposes.

Figure 8 presents a photograph of both types of control units.

4. Power Amplifiers Transfer Function

The power amplifiers used in the engineering model of the discharging system were two Kearfott 3104-A, 16-watt servo amplifiers, which were operated at a carrier frequency of 200 cycles per second.

The gain of these amplifiers, K_a , was adjusted to 1000 during the testing. Consequently, the power amplifier transfer function can be written as

$$\frac{V_a}{V_c} = K_a = 1000 \frac{\text{VOLTS PEAK}}{\text{VOLTS PEAK}} \quad (6)$$

5. High-Voltage Generator Transfer Function

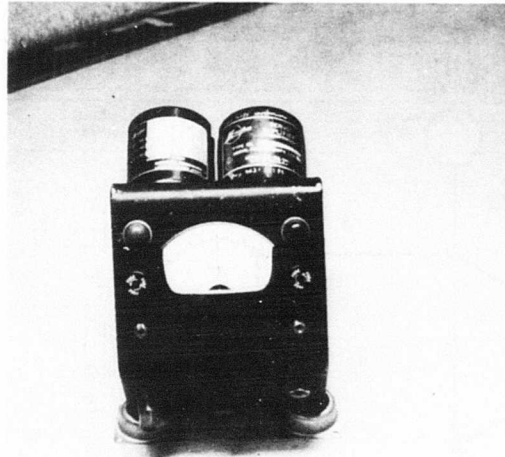
The two lightweight high-voltage generators consisted of a high-voltage transformer and a three-stage rectifier-multiplier circuit, which was designed for air insulation. The schematic diagrams of these units are presented in Figures 9 and 10. Selenium rectifiers were used in the circuit. Additional provisions included suitable resistors to measure and/or record the high-voltage generator voltage as well as the corona point current.

The capacitive nature of the rectifier-multiplier circuit, as well as the characteristics of the high-voltage generator load, produced a relatively low speed of response on this unit. The approximate transfer function of the high-voltage generator was

$$\frac{V_{cp}}{V_a} = \frac{K_g}{1+T_g s} \frac{\text{VOLTS DC}}{\text{VOLTS PEAK}} \quad (7)$$

where K_g is 2500 and T_g is about 0.3 second. A further characteristic of this unit was its asymmetry due to the presence of diode elements in its circuits.

TYPE 1



TYPE 2

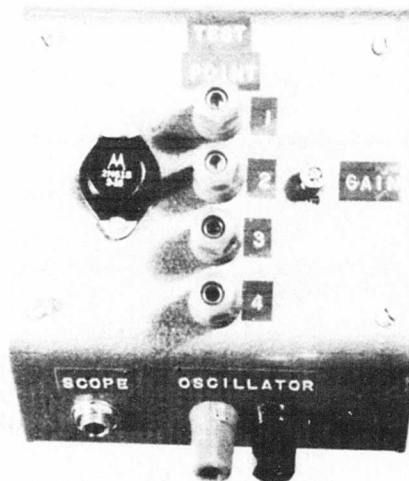
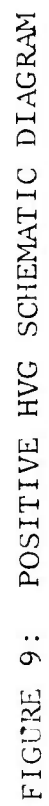


FIGURE 8: TYPE 1 AND TYPE 2 CONTROL UNITS



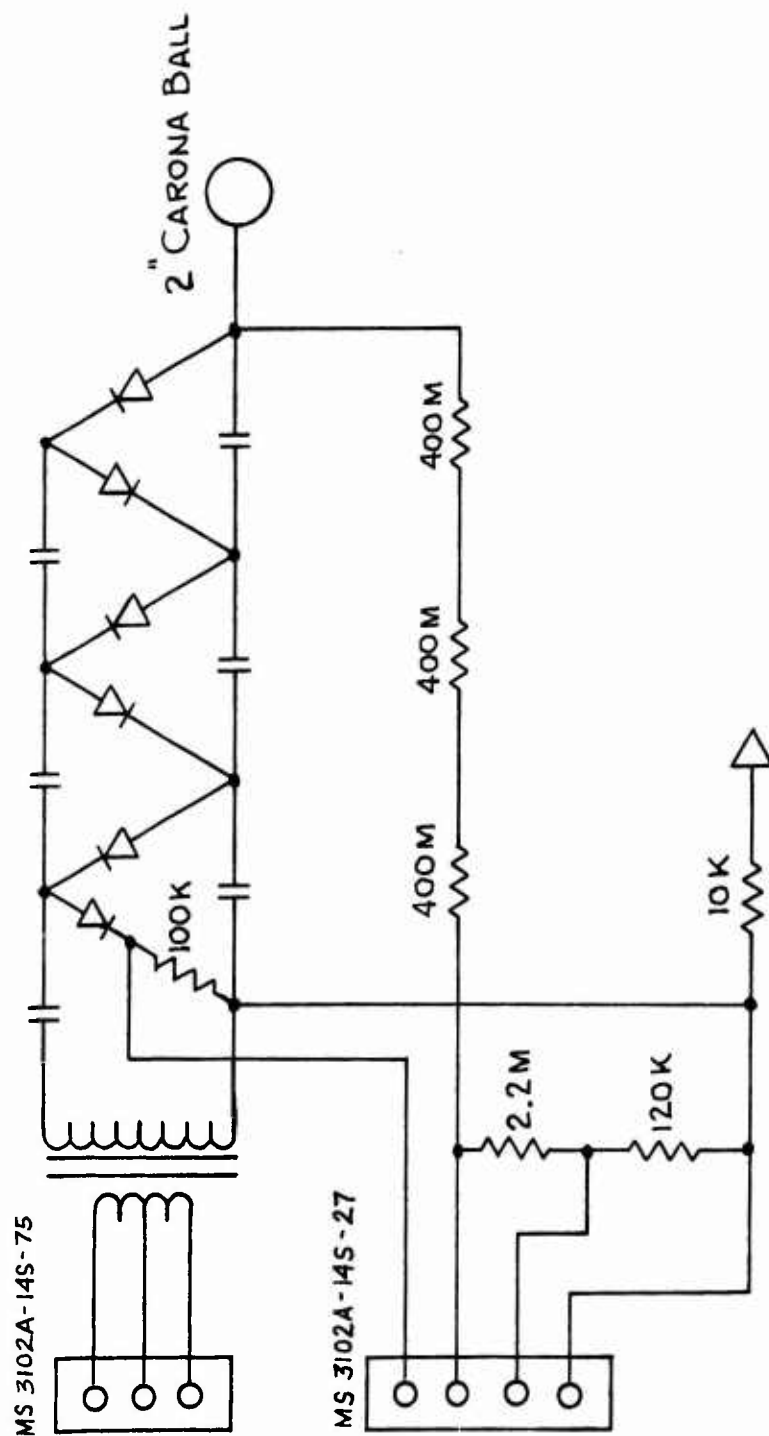


FIGURE 10: NEGATIVE HVG SCHEMATIC DIAGRAM

Because of the nonlinear behavior of the diodes, the time constant of the high-voltage generators has a different value for the increasing and decreasing output voltages.

This asymmetry was considered to be undesirable for the discharging system, as it further complicates the design of the compensation circuits of the discharging devices. Consequently, the design of the high-voltage generator is such that its dynamic characteristics under the actual load are as symmetrical as possible. In fact, this consideration dictated the value of the instrumentation resistor which was used to measure the output voltage of the high-voltage unit.

Figure 11 is a photograph of the high-voltage generator as installed in the tail boom of the test aircraft.

6. Corona Point Probes Transfer Function

It is the function of the corona point probes to transfer into the atmosphere the electrostatic charge which is accumulated by the helicopter. This function is performed by corona action.

The theory of operation of a corona point probe in the atmosphere and the means of measuring its performance have been studied in previous research efforts (References 1 and 2). In addition, a further experimental flight test program was conducted as a part of the present program in order to determine the performance of corona points when installed in the exhaust gas stream of reciprocating and gas turbine helicopter engines. The results of these measurements, which are reported in Section F 1 of this report, confirm and complete the inadequate previous data on the subject.

The performance (current output versus voltage input) of a corona point probe is dependent on a number of design factors: its geometry; the distance from the point to the aircraft surface as related to the strength of the aircraft electrostatic field; and, more important, the relative air

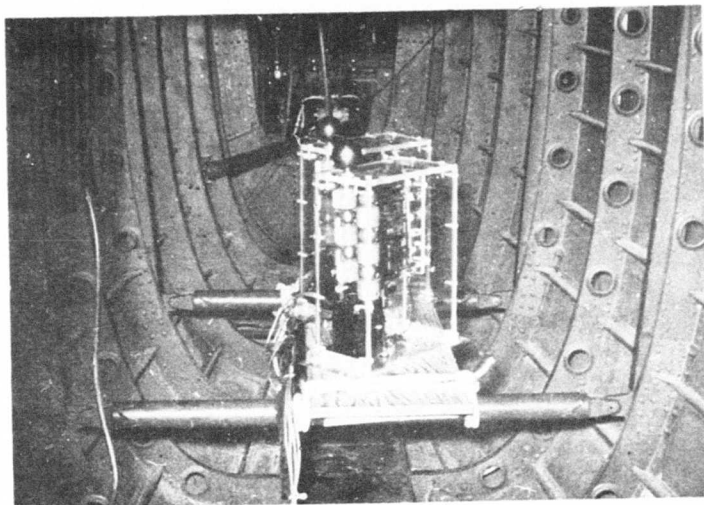


FIGURE 11: HIGH-VOLTAGE GENERATORS INSTALLED IN THE TAIL
OF TEST AIRCRAFT

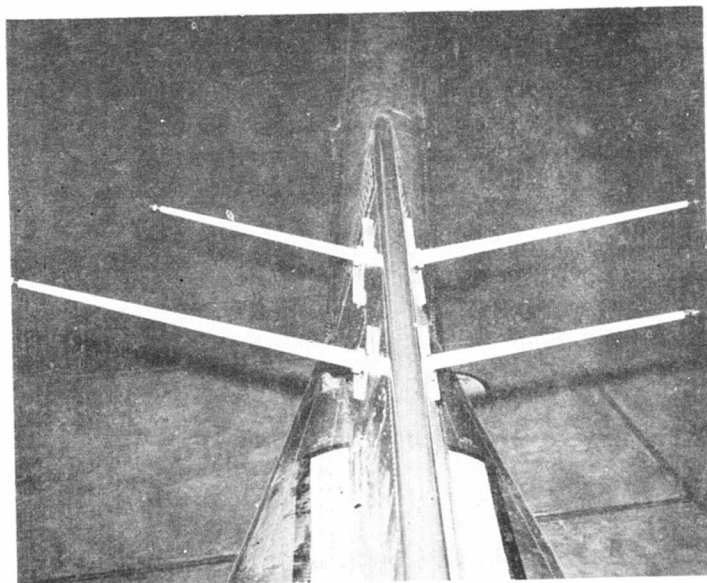


FIGURE 12: CORONA POINT PROBES, VIEW FROM AIRCRAFT ROTOR HUB

speed around the point. These factors are to be considered when determining the configuration of a particular corona discharge probe.

The specifications of the present discharging system called for a maximum discharging current capacity of 50 microamperes. This was achieved by using two corona probes per polarity (the probes were located at the tail section of the H-37 test vehicle used in this program). Figure 12 is a photograph of this installation, which was taken from a location close to the helicopter rotor hub. Figure 13 presents a lateral view of the corona point probes.

The wiring diagram of the corona probe installation is presented in Figure 14. As shown, probes connected to the same generator were installed at opposite sides of the air frame in order to prevent any coupling action between them caused by interaction of their electrostatic fields.

The probes were installed on the tail boom so that they would benefit from the relatively high downwash air speed existing at this location (0.7 to 0.8 rotor radius). The air speed at this zone is probably the maximum attainable along the fuselage. The possibility of a rotor-blade-mounted discharging probe, already explored in Reference 1, was discarded because of its inherent design complexity.

The transfer function of the corona probes can be considered as a constant, as shown in References 1 and 2. The value of the constant for the specific installation used in this program was

$$\frac{I_d}{V_{cp}} = K_{cp} = \frac{5}{6} \times 10^{-9} \frac{\text{AMPERES D C}}{\text{VOLTS D C}} . \quad (8)$$

7. Discharging System Analysis

The dynamic analysis of the electrostatic discharging system is now presented. The transfer functions of the system components, established in the preceding



FIGURE 13: CORONA POINT PROBES INSTALLED ON TEST AIRCRAFT
(SIDE VIEW)

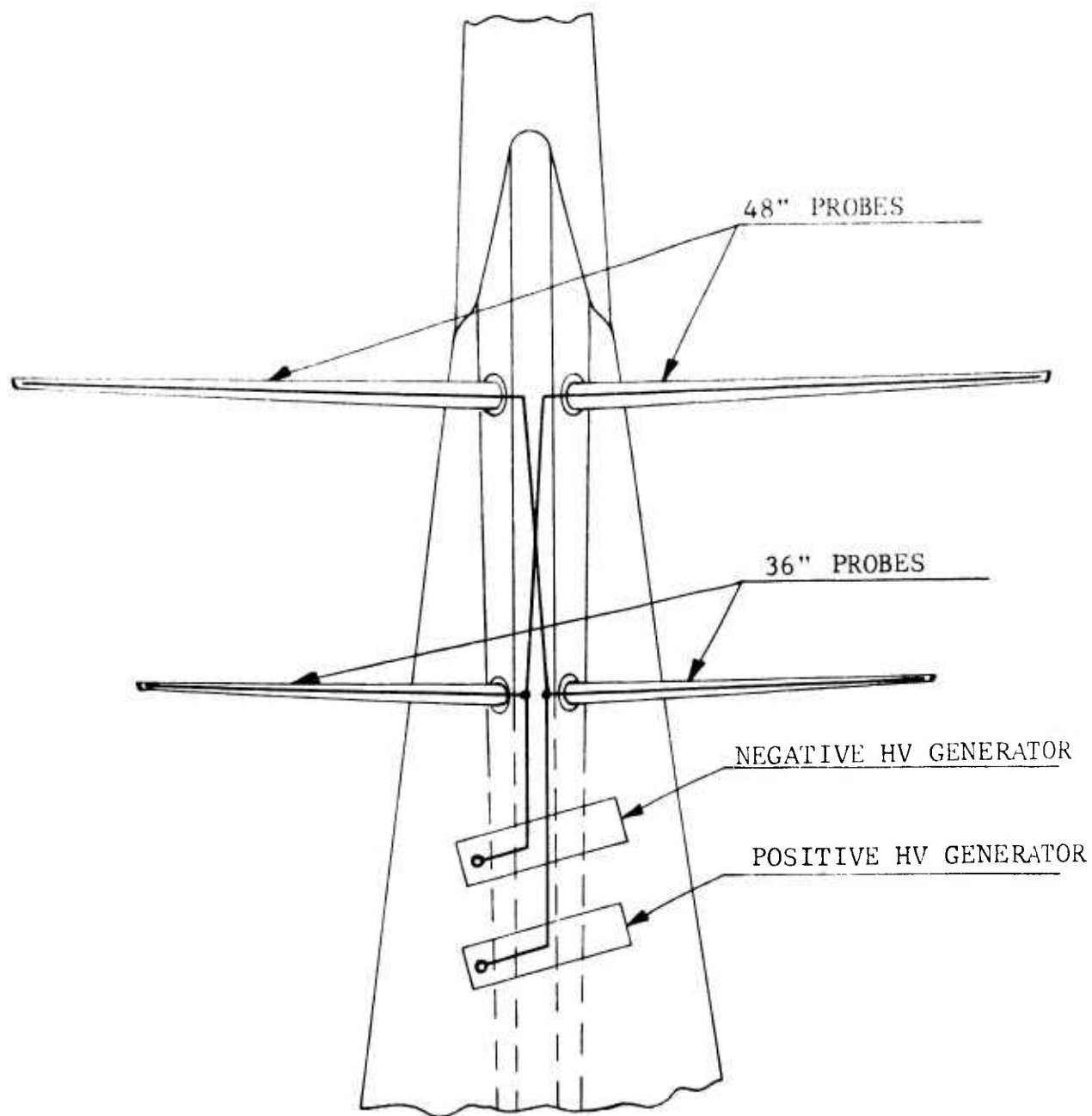


FIGURE 14: CORONA PROBE INSTALLATION WIRING DIAGRAM

section, are the basis of the analysis of the system dynamic behavior. A functional block diagram of the first type of discharging system utilized in this program is presented in Figure 15. The open loop transfer function of this system is

$$F_{o,1} = \frac{I_d}{I_t} = \frac{1}{C_{Hs}} (K_s) (K_{c1}) (K_a) \frac{K_g}{1+T_g s} (K_{cp}). \quad (9)$$

Equation (9) can be written as

$$F_{o,1} = \frac{K}{C_{Hs} (1+T_g s)} \quad (10)$$

where

$$K = K_s K_{c1} K_a K_g K_{cp} \quad (11)$$

The values of the system constants are largely determined by the specifications (listed in Section B) imposed on the discharging system. In accordance with these specifications, the value of V_H must be less than 1,200 volts for natural charging currents, I_n , up to 50 microamperes.

The design helicopter voltage at $I_n = 50$ microamperes was chosen as 1,000 volts. This provided a 200-volt margin for voltage overshoots caused by the system's response to large excitations. In addition, if all dynamic terms are neglected (under steady-state conditions and with V_H held below corona threshold voltage), the system discharging current, I_d , must equal the natural charging current, I_n . It follows that

$$\frac{I_{d,ss}}{V_{H,ss}} = \frac{50 \times 10^{-6}}{10^3} = K_s K_{c1} K_a K_g K_{cp} = K. \quad (12)$$

The values of K_s , K_a , K_g , and K_{cp} are determined by design considerations as described in Section C and are given in Equations (2), (6), (7), and (8) respectively. These equations,

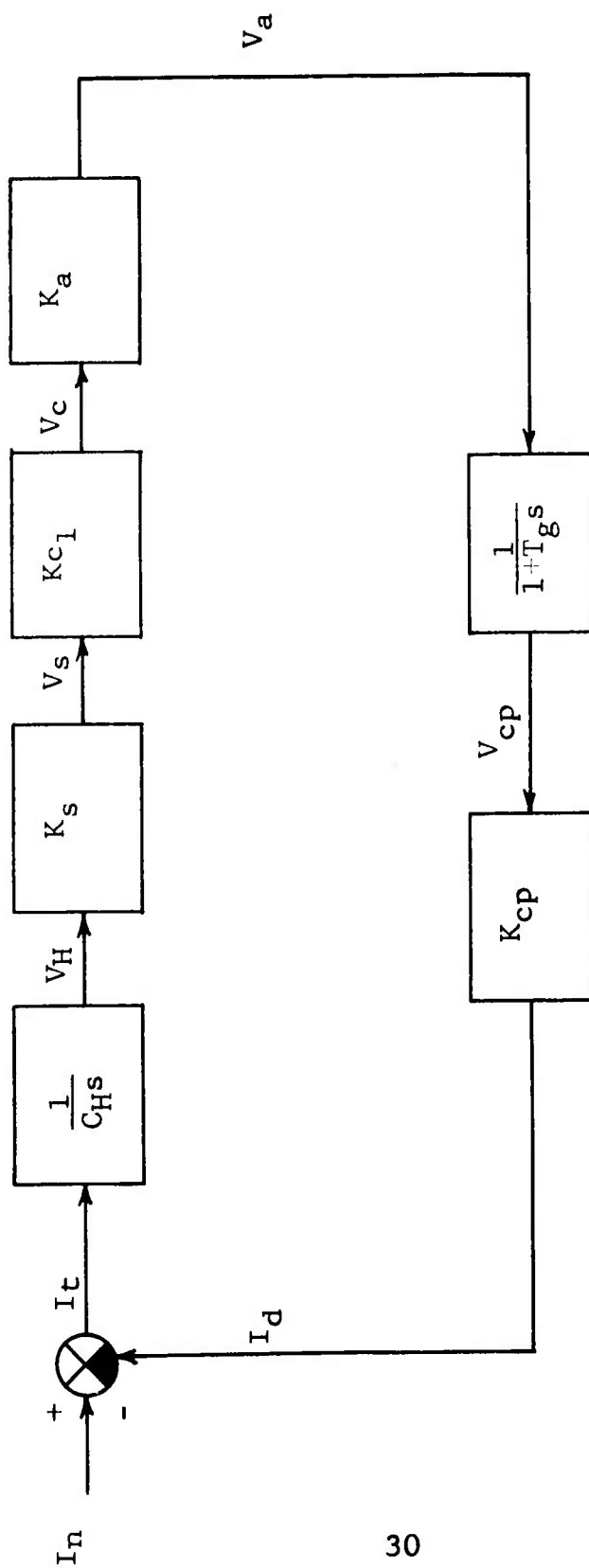


FIGURE 15: TYPE 1 ELECTROSTATIC DISCHARGER FUNCTIONAL BLOCK DIAGRAM

together with Equations (1) and (12), were used to determine the value of K_{c1} as given by Equation (5). The determination of the gain constants of each individual system component leads, in turn, to the system open loop gain, K :

$$K = 5 \times 10^{-8} \quad (13)$$

The closed loop transfer function can be obtained from Equation (10) as follows:

$$F_{c,1} = \frac{I_d}{I_n} = \frac{1}{\frac{C_H T_g}{K} s^2 + \frac{C_H}{K} s + 1} \quad (14)$$

The purpose of the electrostatic discharging system is to maintain the aircraft potential, V_H , below a pre-established level (1,000 volts) for variations of the natural charging current, I_n , within the range of plus or minus 50 micro-amperes. In order to determine the relationship between V_H and I_n , it is convenient to establish a relationship between the discharging current, I_d , and the helicopter voltage, V_H . This is accomplished by multiplying Equations (2), (3), (6), (7), and (8) as follows:

$$\left(\frac{V_s}{V_H}\right)\left(\frac{V_c}{V_s}\right)\left(\frac{V_a}{V_c}\right)\left(\frac{V_{cp}}{V_a}\right)\left(\frac{I_d}{V_{cp}}\right) = K_s K_{c1} K_a \frac{K_g}{1+T_g s} K_{cp} \quad (15)$$

Applying Equation (11) to Equation (15) and simplifying,

$$\frac{I_d}{V_H} = \frac{K}{1+T_g s} ; \quad (16)$$

and from Equations (14) and (16),

$$\frac{V_H}{I_n} = \frac{1 + T_g s}{K \left(\frac{C_H T_g s}{K} s^2 + \frac{C_H}{K} s + 1 \right)} \quad (17)$$

The characteristics of the discharging system described by Equation (17) can be analyzed by studying the response of the system to a step function of magnitude K_1 . The operational representation of this step function is

$$I_n = \frac{K_1}{s} \quad (18)$$

The time history of the helicopter voltage after the application of such an input to the system is

$$V_H = K_s \frac{K_1 (1 + T_g s)}{\left(\frac{C_H T_g}{K} s^2 + \frac{C_H}{K} s + 1 \right)} \quad (19)$$

The time-dependent equation corresponding to Equation (19) can be found by determining its inverse Laplace transform

$$V_H = \frac{K_1}{K} \left\{ 1 + \frac{1}{\sqrt{1 - \zeta^2}} \left[1 - 2 T_g \zeta \omega_1 + T_g^2 \omega_1^2 \right]^{\frac{1}{2}} \cdot \left[e^{-\zeta \omega_1 t} \sin(\omega_1 \sqrt{1 - \zeta^2} t + \psi) \right] \right\} \quad (20)$$

where

$$\zeta = \frac{1}{2} \left(\frac{C_H}{K T_g} \right)^{\frac{1}{2}} \quad (21)$$

$$\omega_1 = \left(\frac{K}{C_H T_g} \right)^{\frac{1}{2}} \quad (22)$$

$$\psi = \tan^{-1} \frac{T_g \omega_1 \sqrt{1 - \zeta^2}}{1 - T_g \zeta \omega_1} - \frac{\tan^{-1} \sqrt{1 - \zeta^2}}{-\zeta} \quad (23)$$

Parameters ζ , ω_1 , and ψ (defined by Equations (21), (22),

and (23)) are respectively the system damping ratio, the system natural frequency, and the phase angle of the helicopter voltage with respect to the time of occurrence of the input function.

The values of the natural frequency, ω_1 , and phase angle, ψ , are of relatively little importance for the evaluation of the behavior of the electrostatic discharging system. The value of the damping ratio, ζ , on the other hand, provides information on the system stability and speed of response characteristics. Equation (21) shows that the damping ratio is a function of three parameters: the helicopter capacitance, C_H ; the constant, K , defined in Equation (11); and the high-voltage generator time constant, T_g . The value of C_H is, of course, determined by the aircraft size and geometry; the value of K is determined by the system specifications, as explained above in this section. Consequently, in order to increase the system damping ratio, the value of T_g must be made as small as possible. This is, of course, limited by design considerations. A value of $T_g = 0.3$ is about the lowest value that can be attained without sacrificing other design requirements of the high-voltage power supply. Table 1 gives the values of the system natural frequency and damping ratio for values of the high-voltage generator time constant when the system gain setting (K_{c1}) is 8×10^3 . These values range from 0.5 to 0.04 second. Figure 16 presents the relationship between the natural frequency, ω_1 , and the high-voltage generator time constant, T_g , for the five gain settings utilized in the Type 1 control unit. It should be noted that an increase in system gain setting, for a constant high-voltage generator time constant, results in an increase of the natural frequency. This fact was utilized for the experimental verification of the effect of system damping ratio on the system dynamics.

TABLE 1

NATURAL FREQUENCY (ω_1) AND DAMPING RATIO (ζ)
 OF THE DISCHARGING SYSTEM AS A FUNCTION OF THE
 HIGH-VOLTAGE GENERATOR TIME CONSTANT (T_g)
 ($K_{c1} = 8 \times 10^3$)

T_g Seconds	ω_1		ζ Damping Ratio
	Radians per Second	Cycles per Second	
0.5	10	1.59	0.1
0.25	14.1	2.22	0.141
0.1	22.4	3.55	0.224
0.05	31.8	5.05	0.318
0.04	35.3	5.60	0.353

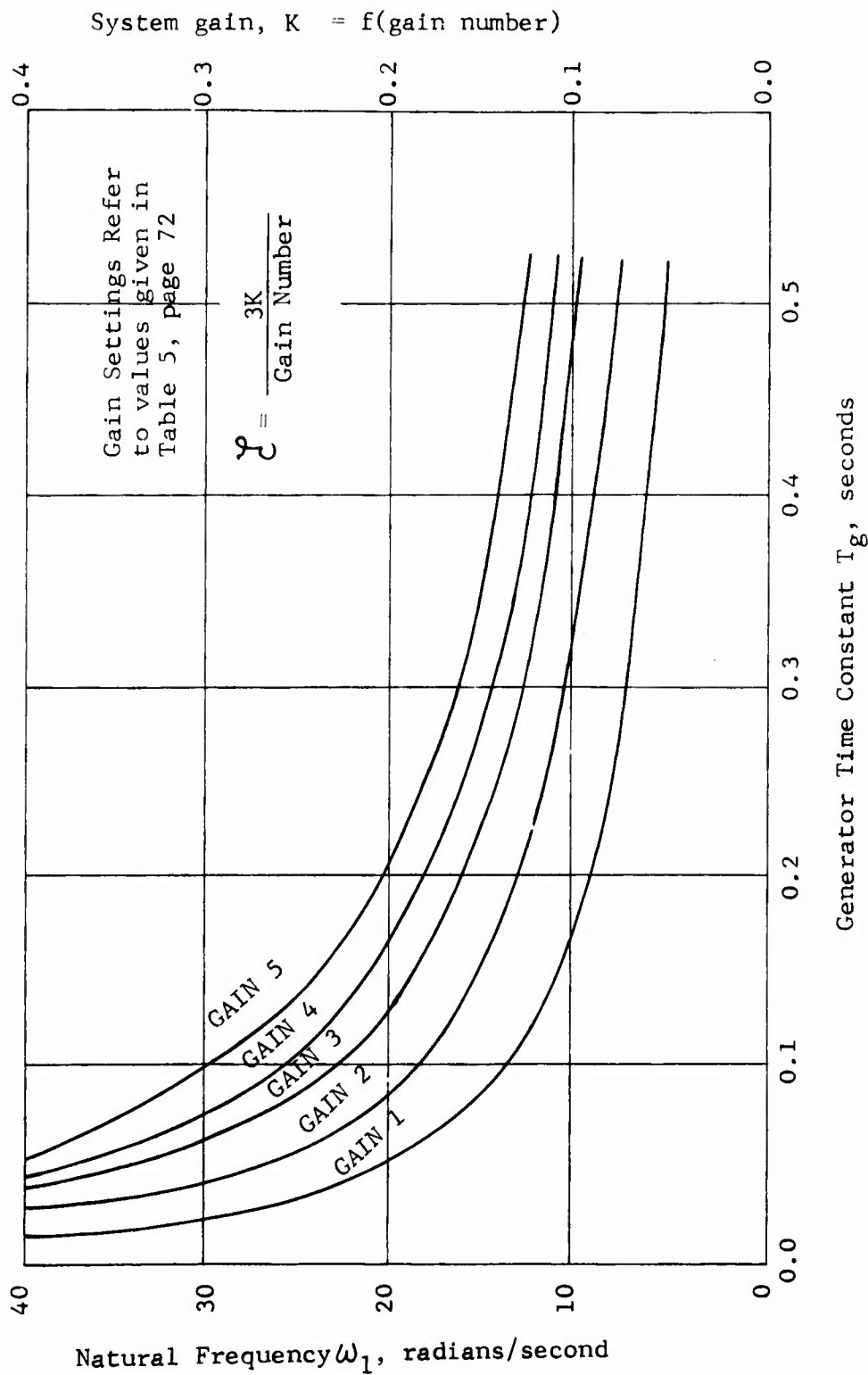


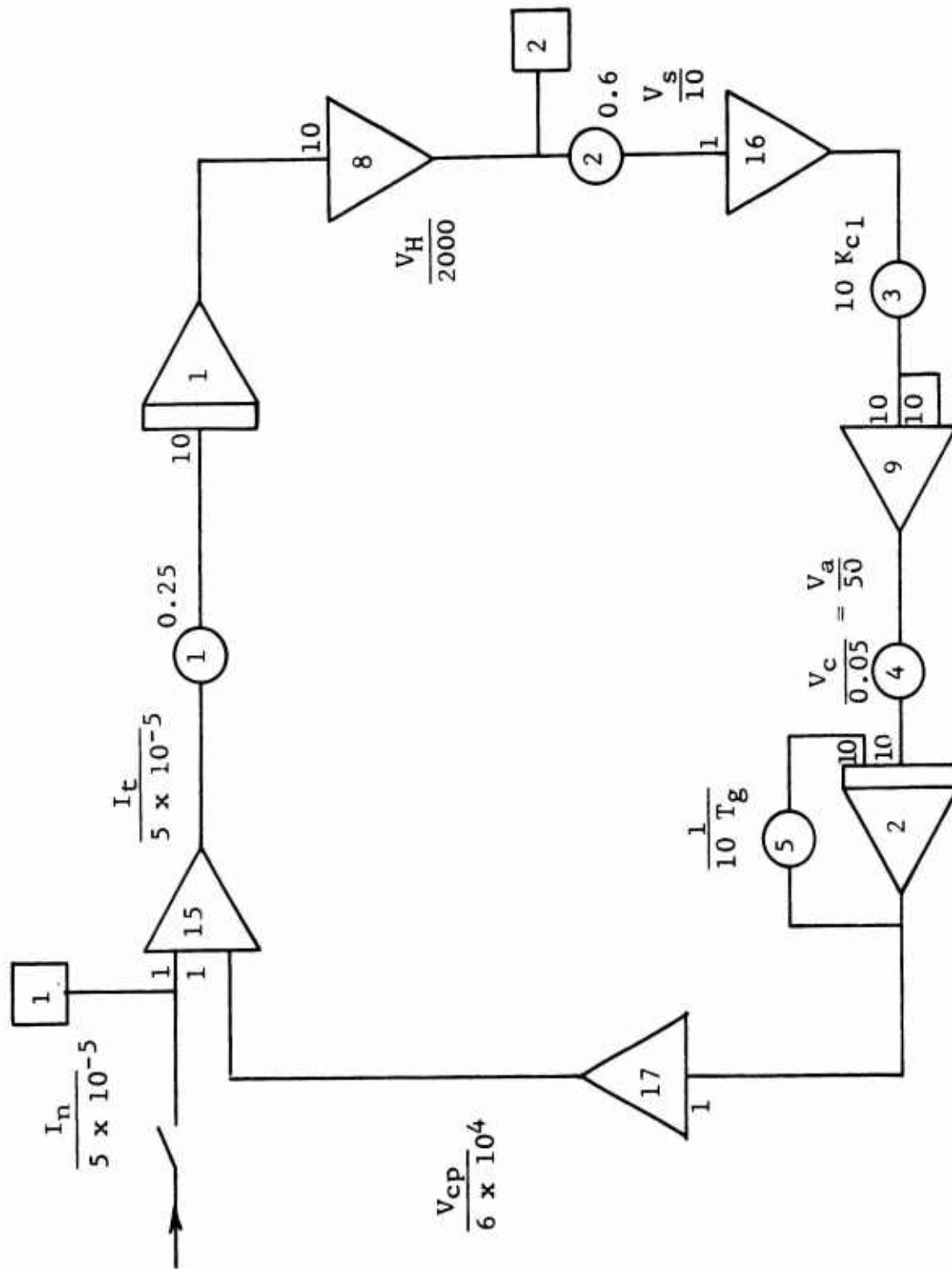
FIGURE 16: NATURAL FREQUENCY (ω_1) AND DAMPING RATIO (\mathcal{L}) OF THE DISCHARGING SYSTEM AS A FUNCTION OF THE HIGH-VOLTAGE GENERATOR TIME CONSTANT (T_g)

In order to evaluate the effect of the system damping ratio on the system response to a step input, the discharging system was programmed on an analogue computer. Figure 17 shows the computer diagram of the analogue simulation. The analogue computer analysis is presented in Appendix A. Figure 18 reproduces the computer-obtained time histories of the helicopter voltage, V_H , for several values of the constant, T_g .

It is seen that the system damping for high values of T_g is not sufficient. A damping ratio on the order of 0.35 would be satisfactory. However, this requires a high-voltage generator time constant, T_g , of 0.04 second, which is by far smaller than that physically attainable with reasonable amounts of input power.

A possible method by which to test the system operation with varying damping ratios using a high-voltage generator with a time constant of 0.3 second consists of introducing variations to the system gain, K . This becomes clear by inspecting Equation (21). Certainly, if K is decreased to produce an increase of the damping ratio, the system gain will be correspondingly decreased and the helicopter voltage for any discharging current level will be accordingly higher. This, however, is acceptable during a discharger flight test program. The analogue simulation of such a condition was performed in the analogue computer set-up. Figure 18 reproduces the computer traces obtained for five values of the system gain, K_c . These traces are directly comparable with flight test traces obtained by setting the system gain at corresponding values.

A discharging device having the characteristics referred to in the preceding discussion was built as part of this program. The control unit of this discharger has been referred to as Type 1 control unit in Section C 3. This control unit was used in the Phase 7 flight test program conducted at Fort Rucker, Alabama. The results of these flight tests were in very good agreement with the analytical and computer results mentioned above. More detailed discussion of the correlation of test data with the theory is presented in Sections E and F. It suffices here to note that this agreement was considered as supporting the soundness of the basic assumptions utilized in the system analysis.



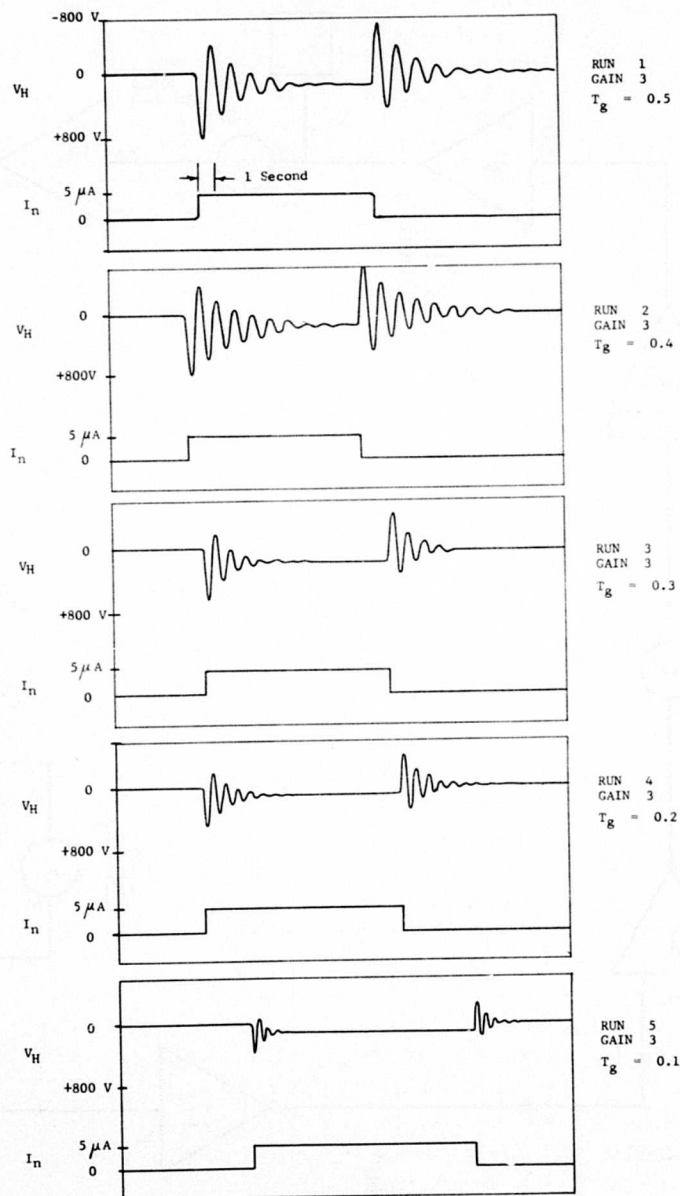


FIGURE 18: V_H AS A FUNCTION OF TIME, t , FOR VARIOUS VALUES OF T_g (COMPUTER TRACES)

In order to achieve satisfactory damping with the Type 1 control unit, the gain of the system, K , would have to be lower than that required to meet the discharging system specifications. To overcome this incompatibility, the Type 2 control unit was designed. The block diagram of the discharging system using a Type 2 control unit is presented in Figure 19. The Type 2 control unit includes an RC network having a transfer function as follows:

$$\frac{V_c}{V_s} = K_{c2} \frac{1+T_1s}{1+T_cs} \quad (24)$$

where

$$K_{c2} = K_{c1} \quad (25)$$

$$T_1 = T_g \quad (26)$$

With the Type 2 control unit in the loop, the discharging system open loop transfer function is

$$F_{o,2} = \frac{1}{C_H s} (K_s) K_{c1} \frac{1+T_g s}{1+T_c s} (K_a) \frac{K_g}{1+T_g s} K_{cp} \cdot \quad (27)$$

Applying Equation (11) and simplifying, there results

$$F_{o,2} = \frac{K}{C_H s (1+T_c s)} = \frac{I_d}{I_t} \cdot \quad (28)$$

Equation (28) is similar to Equation (10). The only difference between these two equations is the substitution of T_g in Equation (10) by T_c in Equation (28). Consequently, the closed loop transfer function and response to a step input on a Type 2 system can be written by substituting T_c by T_g in Equations (14), (19), and (20) as

$$F_{c,2} = \frac{1}{\frac{C_H T_c}{K} s^2 + \frac{C_H}{K} s + 1} = \frac{I_d}{I_n} \cdot \quad (29)$$

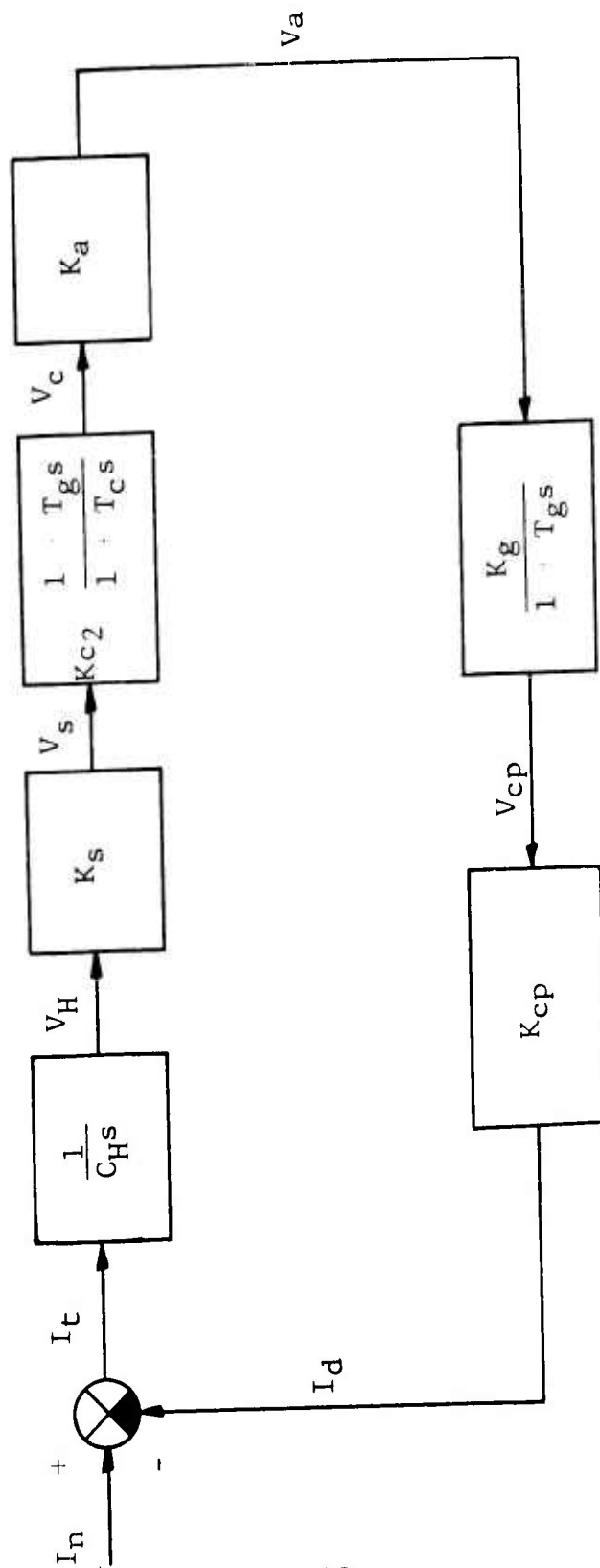


FIGURE 19: TYPE 2 ELECTROSTATIC DISCHARGER FUNCTIONAL BLOCK DIAGRAM

$$V_H = \frac{K_1 (1 + T_c s)}{K_s \left(\frac{C_H T_c}{K} s^2 + \frac{C_H}{K} s + 1 \right)} \quad (30)$$

and

$$V_H = \frac{K_1}{K} \left\{ 1 + \frac{1}{\sqrt{1 - \zeta^2}} \left[1 - 2 T_c \zeta \omega_1 + T_c^2 \omega_1^2 \right]^{\frac{1}{2}} \cdot \left[e^{-\zeta \omega_1 t} \sin(\omega_1 \sqrt{1 - \zeta^2} t + \psi) \right] \right\} \quad (31)$$

Parameters of Equation (31) are defined by

$$\zeta = \frac{1}{2} \left(\frac{C_H}{K T_c} \right)^{\frac{1}{2}} \quad (32)$$

$$\omega_1 = \left(\frac{K}{C_H T_c} \right)^{\frac{1}{2}} \quad (33)$$

and

$$\psi = \tan^{-1} \frac{T_c \omega_1 \sqrt{1 - \zeta^2}}{1 - T_c \zeta \omega_1} - \tan^{-1} \frac{\sqrt{1 - \zeta^2}}{-\zeta} \quad (34)$$

The value of the damping ratio, ζ , in a discharging system using the Type 2 control unit is represented by Equation (32). For specified values of C_H and K , the value of ζ can be adjusted by using proper values of T_c . The possible range of adjustment is quite wide, although the ratio between T_c and T_g must be kept within reasonable limits to avoid excessive high-frequency noise amplification inherent to the transfer function of the Type 2 control unit. A value of $T_c = 0.03$ was used in the present program with satisfactory results. The value corresponds to a system damping ratio of near 0.4, which is adequate as shown in the corresponding traces in Figures 18 and 20.

The discharging system with the Type 2 control unit was tested in flight in the test program conducted at Fort Greely, Alaska. The dynamic characteristics of the system were in

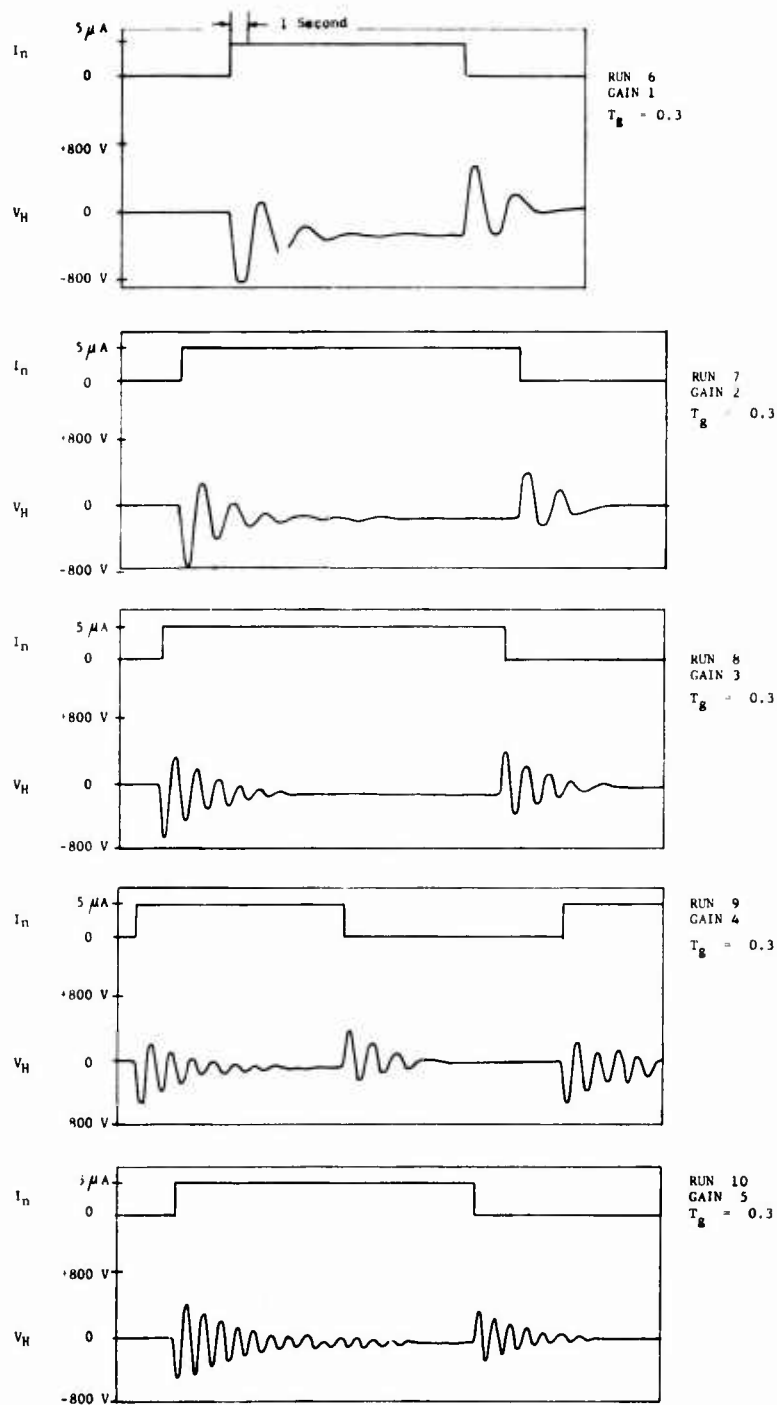


FIGURE 20: V_H AS A FUNCTION OF TIME, t , FOR VARIOUS VALUES K_C (COMPUTER TRACES)

good agreement with those predicted by theory, as is further discussed in Sections E and F of the Technical Discussion.

D. INSTRUMENTATION DESCRIPTION

The instrumentation used in this program was designed to be installed on a special bench, which was capable of being taken from one test vehicle to another with a minimum of effort. The test bench served also as a place for instrument storage during the shipments between test sites. Two shock-mounted instrument shelves were provided, and the instruments were fastened to these shelves with simple bungee chord straps.

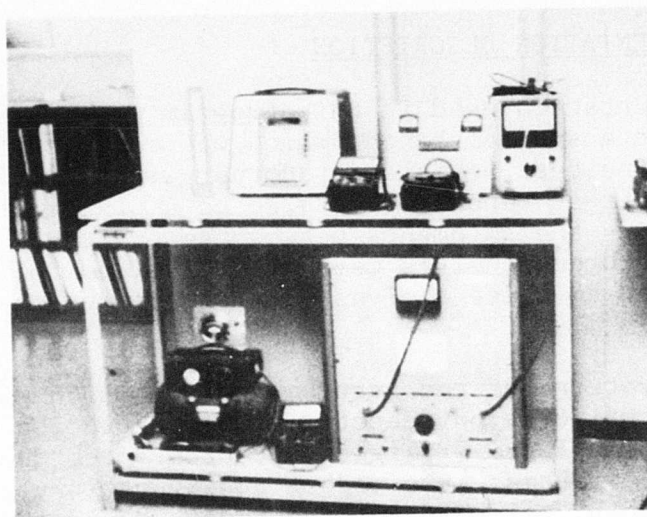
Two configurations of the instrumentation bench were used. The first configuration, denoted as Configuration A, was used during the Phase 7 flight test program conducted at Fort Rucker, Alabama; the second configuration, denoted as Configuration B, was used for the Phases 9 and 10 flight tests at Fort Greely, Alaska, and Edwards Air Force Base, California, respectively. Photographs of both configurations of the test bench are shown in Figure 21.

The principal difference between the two configurations consists of the replacement of the high-voltage generator and terminal corona balls by a group of instruments consisting of a cathode ray oscilloscope, a low-voltage D-C power supply, and an audio frequency generator. In addition, the millivoltmeter and the barometer used in the first configuration to determine the characteristics of the engine exhaust gas (phase 6) were eliminated on the second configuration to allow more room for the new control unit of the electrostatic discharger.

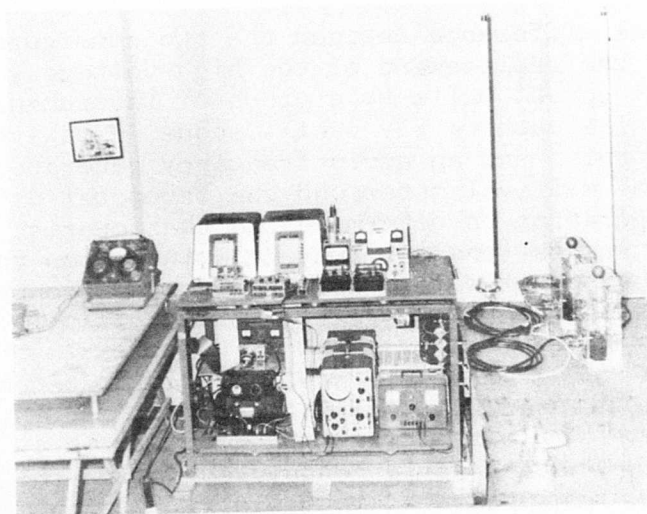
The schematic diagram of the instrumentation bench is presented in Figure 22.

The recording channel assignments used during the flight test programs are presented in Table 2. Analogue Channel 1 was used for three different purposes, depending on the nature of each test flight. A three-position toggle switch on the control panel was used as mode selector for Channel 1.

Two double channel recorders were used in the program. In order to synchronize the records obtained in both instruments, a sync unit was designed and built. This unit provided timing



CONFIGURATION A



CONFIGURATION B

FIGURE 21: INSTRUMENTATION TEST BENCH, CONFIGURATIONS A AND B

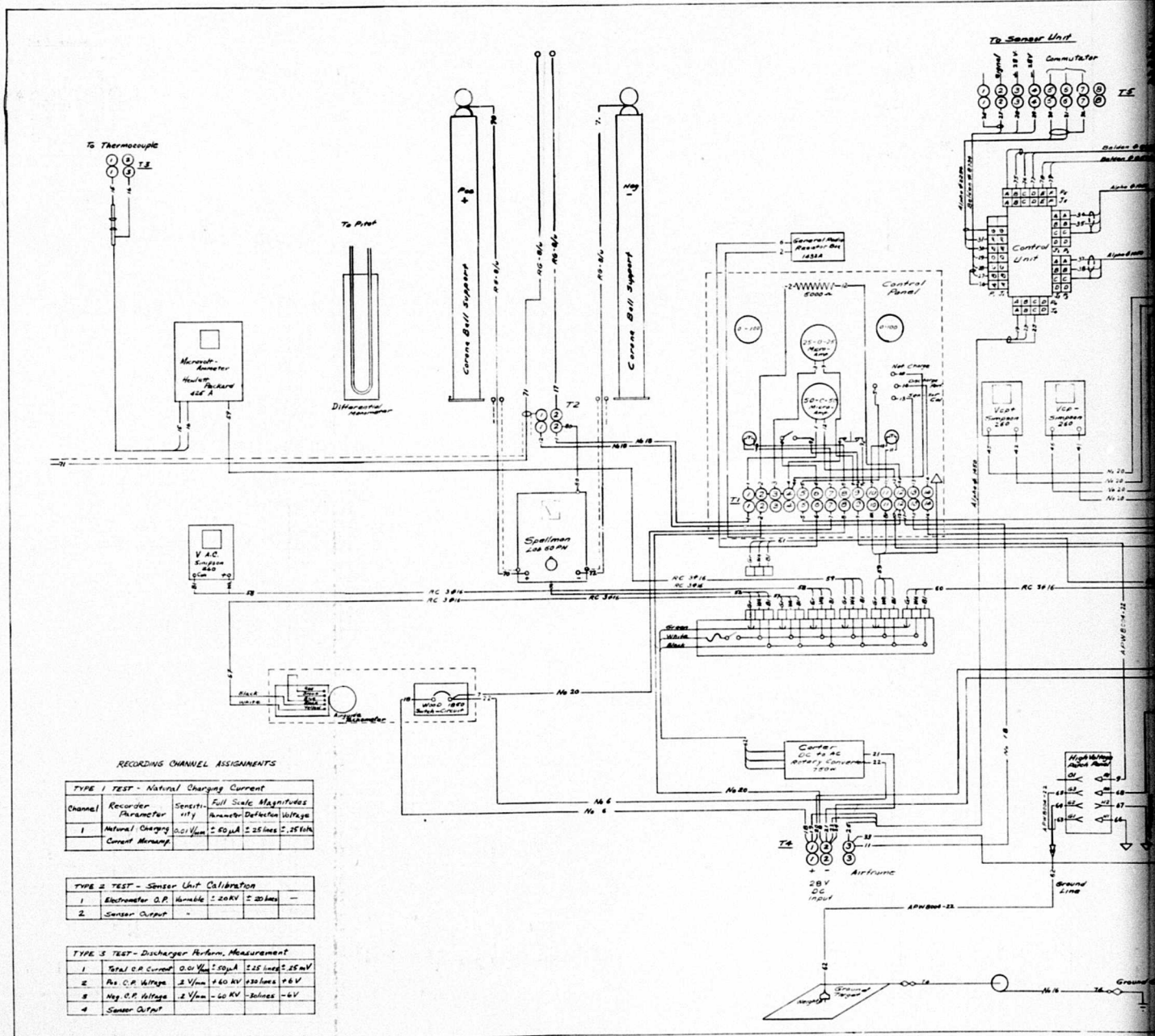


FIGURE 22: INSTRUMENTATION BENCH SCHEMATIC WIRING DIAGRAM

TABLE 2
RECORDING CHANNEL ASSIGNMENTS

<u>ANALOGUE CHANNELS</u>		<u>Full-Scale Values</u>			
Channel	Recorder	Parameter	Sensitivity	Parameter	Deflection Voltage Lines
1	A	Nat. Charg. Current 0.01 V/M Electrometer Output Variable Total C.P. Current 0.01 V/M		$\pm 50 \mu A$	± 25
				$\pm 20 KV$	± 20
				$\pm 50 \mu A$	± 25
2	A	Sensor Output	-	-	-
3	B	Positive C.P. Vtg. 0.2 V/M		+ 60 KV	+ 6
4	B	Negative C.P. Vtg. 0.2 V/M		- 60 KV	- 6
<u>EVENT CHANNELS</u>					
A1	A	Sync-Timer			
A2	A	Discharger Power Status (ON-OFF)			
B3	B	Sync-Timer			
B4	B	Polarity Status (POS-NEG)			

*NOTE: This mode of operation of Channel 1 was inoperative during the program due to high transformer-induced noise at the point of signal pickup.

pulses to an event channel in each recorder. The pulse sequence was initiated only when both recording paper motors were activated. A photograph of this device is presented in Figure 23.

E. EXPERIMENTAL PROCEDURE AND RESULTS

The results obtained in the experimental phases of this program are reported in this section. A brief description of the experimental procedure followed to obtain the data is also given herein.

In order to systematize the presentation of the experimental information, the data will be broken down into four parts as follows:

1. Engine-exhaust-mounted corona point performance data, obtained during program Phase 6.
2. Type 1 discharger performance data, obtained during program Phase 7.
3. Type 2 discharger performance data, obtained during program Phase 9.
4. Discharging system radio interference measurements, obtained during program Phases 5 and 10.

The program phases are defined in Section A of the Technical Discussion.

1. Engine-Exhaust-Mounted Corona Point Performance

Two types of aircraft were used as test vehicles during this program: Sikorsky CH-37 Mojave helicopter, powered by two Pratt & Whitney Model R-2800, 2100-horsepower reciprocating engines; and the Boeing-Vertol CH-47A Chinook helicopter, powered by two Lycoming Model T-55-L-5 1940-horsepower gas turbine engines.

Both of these aircraft being twin-engined, the high-voltage corona point was installed in the exhaust of one engine and the gas characteristics were determined at the corresponding location in the second engine exhaust.

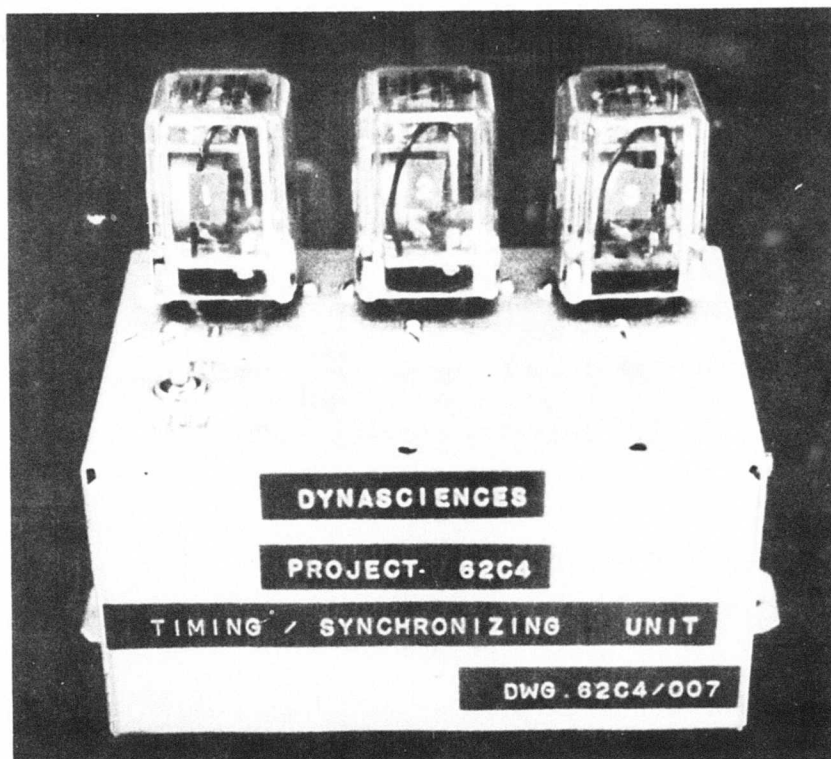


FIGURE 23: TIME-SYNC UNIT

Figures 24 and 25 are photographs of the engine exhaust probes installed in the CH-37 and CH-47A helicopters, respectively.

The natural charging current at the test site was recorded immediately prior to each test flight and several times during each series of measurements, in order to ascertain repeatability.

A simplified schematic diagram of the test instrumentation used during this part of the program is presented in Figure 26. This figure is also utilized to define the symbols and polarities corresponding to the data presented herein. The measured parameters were:

- I_g = current flow through the ground line.
- I_n = natural charging current equal to I_g , when the high-voltage power supply voltage is zero.
- I_t = total amount flowing through the high-voltage power supply.
- V_{cp} = high-voltage power supply output voltage, or corona point voltage.

The measurement of these parameters permits the calculation of the value of the discharging current, I_d , by using the following equation:

$$I_d + I_n - I_g = 0. \quad (35)$$

I_d is the significant parameter in determining the discharging performance of the system under test. It should be noted that the value of the natural charging current, I_n , was recorded at the beginning of each test flight, and then considered as a constant during the rest of the data-taking period. The validity of this procedure is substantiated in Reference 2 and is further verified in the present program.

The value of I_g was measured with a mirrored microammeter as well as recorded by an oscillograph. Both values (read and recorded) were found to be in excellent agreement; therefore, only one is given in the subsequent tables and charts.

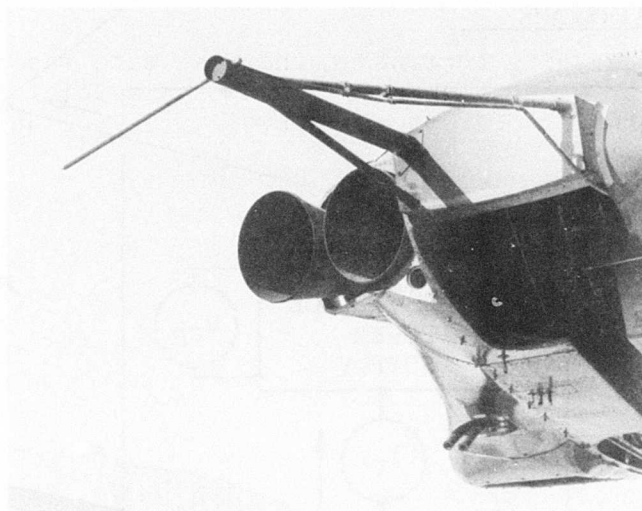
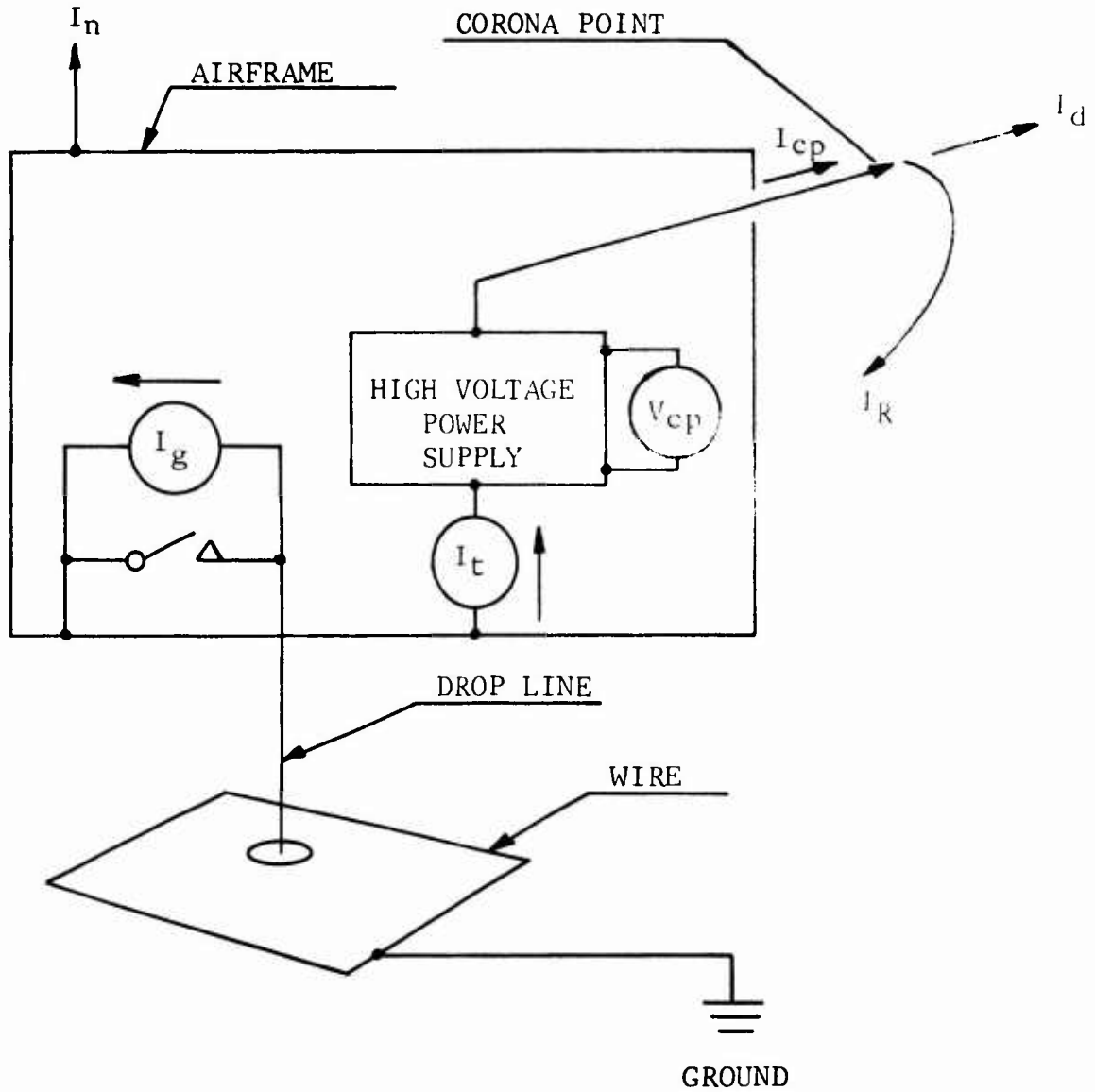


FIGURE 24: EXHAUST PROBE
INSTALLATION ON CH-37
AIRCRAFT



FIGURE 25: EXHAUST PROBE
INSTALLATION ON CH-47A
AIRCRAFT



Arrows indicate direction of electron flow.
Therefore, a positive value of I_n results in
a positively charged helicopter

FIGURE 26: CURRENT POLARITY CONVENTION

The results obtained during this phase of the program are presented in Tables 3 and 4. These tables also include the calculated values of the discharging current, I_d . The value of this parameter (I_d) is plotted against V_{cp} in Figures 27 and 28. In addition, Tables 3 and 4 present the environmental conditions (gas temperature and speed) at the three corona point locations used during the test program.

By inspecting Table 3, which contains data taken on the CH-37 aircraft, it can be observed that the recorded value of I_t corresponds very closely to the value of I_d calculated by using Equation 35. It follows that practically all the current flow through the high-voltage power supply, and obviously through the corona probe, was being blown away from the air frame by the action of the flowing exhaust. This means that the recirculation current I_R , shown in Figure 26, is very close to zero. The result confirms the data presented in Reference 2 (Table 2), which was obtained with the same aircraft and corona point installation.

The data presented in Table 4, which were obtained with the CH-47 aircraft, indicate that a quite different situation exists. The values of I_t at high voltages are significantly larger than those calculated for I_d by using Equation 35. This indicates that a recirculation current I_R flowed between the high side of the power supply (or the probe) and the air frame.

This current flow was found to be due to corona current flowing between the mounting bracket of the plastic tube used to insulate the probe rod and the probe itself. A laboratory test set up described in Figure 29 was prepared and tested under a no-wind condition. The results obtained in this test are also included in Figure 29.

The presence of corona currents between the probe rod mount and the bracket was conclusively proved. These currents are of the same magnitude as the difference between I_t and I_d indicated in Table 4.

A comparison of the performance of exhaust-mounted points and fuselage-mounted points indicates little advantage of the former configuration. Therefore, it was decided to use corona points installed on the tail fin of the CH-37 test aircraft during the remaining phases of the program.

TABLE 3
ENGINE-EXHAUST-MOUNTED CORONA POINT PERFORMANCE DATA,
CH-37 AIRCRAFT (MOJAVE)

Natural Charging Current $I_n = +3 \mu A$
Gross Weight: 30,000 to 32,000 lbs.
Altitude: 15 to 20 feet.

Corona Point Voltage, Kilovolts	Station 48" *			Station 36" *			Station 24" *		
	Recorded		Calculated	Recorded		Calculated	Recorded		Calculated
	I_g	I_t	I_d	I_g	I_t	I_d	I_g	I_t	I_d
	A	A	A	A	A	A	A	A	A
0	+3	0	0	+3	0	0	+3	0	0
+20	0,+1	-2	-2, -3	0,+1	-2	-1,-3	0,-2	-3	-3,-5
+30	-2,-4	-6	-5, -7	-3,-4	-6	-6,-7	-3,-7	-8	-6,-10
+40	-7,-9	-11	-10,-12	-7,-10	-11	-10,-13	-9,-12	-13	-17,-15
+50	-11,-14	-16	-14,-17	-12,-15	-16	-15,-18	-14,-16	-18	-17,-19
+60	-15,-21	-20	-18,-24	-16,-23	-22	-19,-26	-19,-25	-25	-27,-28
-20	+4,+6	-	+1, +3	+4,+6	-	+1,+3	+5,+8	-	+2,+4
-30	+8,+10	+6	+5, +7	+8,+11	+5	+5,+8	+10,+12	+6	+7,+9
-40	+13,+15	+10,+11	+10,+12	+14,+16	+12	+11,+13	+16,+18	+11	+11,+15
-50	+18,+21	+15,+16	+15,+18	+19,+22	+15	+16,+19	+19,+22	+17	+16,+19
-60	+21,+26	+20	+18,+23	+23,+29	+25	+20,+26	+24,+31	+25	+21,+28

Gas Static Temperature, ° F **	153°	220°	276°
Gas Speed, fps.	125	159	184

* Distance from the exhaust stack nozzle to the high-voltage probe, in inches.
** Measured with iron-constantan thermocouple exposed to the gas stream

TABLE 4
ENGINE-EXHAUST-MOUNTED CORONA POINT PERFORMANCE DATA,
CH-47A AIRCRAFT (CHINOOK)

Natural Charging Current: +2 μ A.			Gross Weight: 31,500 lbs.			Altitude: 20 to 25 feet			
Corona Point Voltage, Kilovolts	Station 48" *			Station 36" *			Station 24" *		
	Recorded		Calculated I _d A	Recorded		Calculated I _d A	Recorded		Calculated I _d A
	I _g A	I _t A		I _g A	I _t A		I _g A	I _t A	
0	+2	0	0	+2	0	0	+2	0	0
+20	-1	-15	-3	0	-17	-2	-2	-24	-4
+30	-2, -4	-24	-4, -6	5	-35	-7	-5	-35	-7
+40	-9, -10	-35	-11, -12	-9	-41	-11	-12, -13	50	-14, -15
+50	-10, -14	-45	-12, -16	-14, -16	50	-16, -18	-17	50	-19
+60	-17, -21	50	-19, -23	-22, -24	50	-24, -26	-25, -26	50	-27, -28
-20	+4	+14	+2	+4	+16	+2	+5	+24	+3
-30	+7, +8	+25	+5, +6	+9, +10	+34	+7, +8	+10	+36	+8
-40	+13	+35	+11	+14	+42	+12	+16, +17	+51	+14, +15
-50	+18, +19	+47	+16, +17	+20, +21	50	+18, +19	+20	50	+18
-60	+22, +25	50	+20, +23	+27, +28	50	+25, +26	+28, +30	50	+26, +28

Gas Static
Temp. ° F **

772

748

748

Gas Speed
fps.

224

226

256

* Distance from the exhaust stack nozzle to the high-voltage probe, in inches.
** Measured with ion-constantan thermocouple exposed to the gas stream.

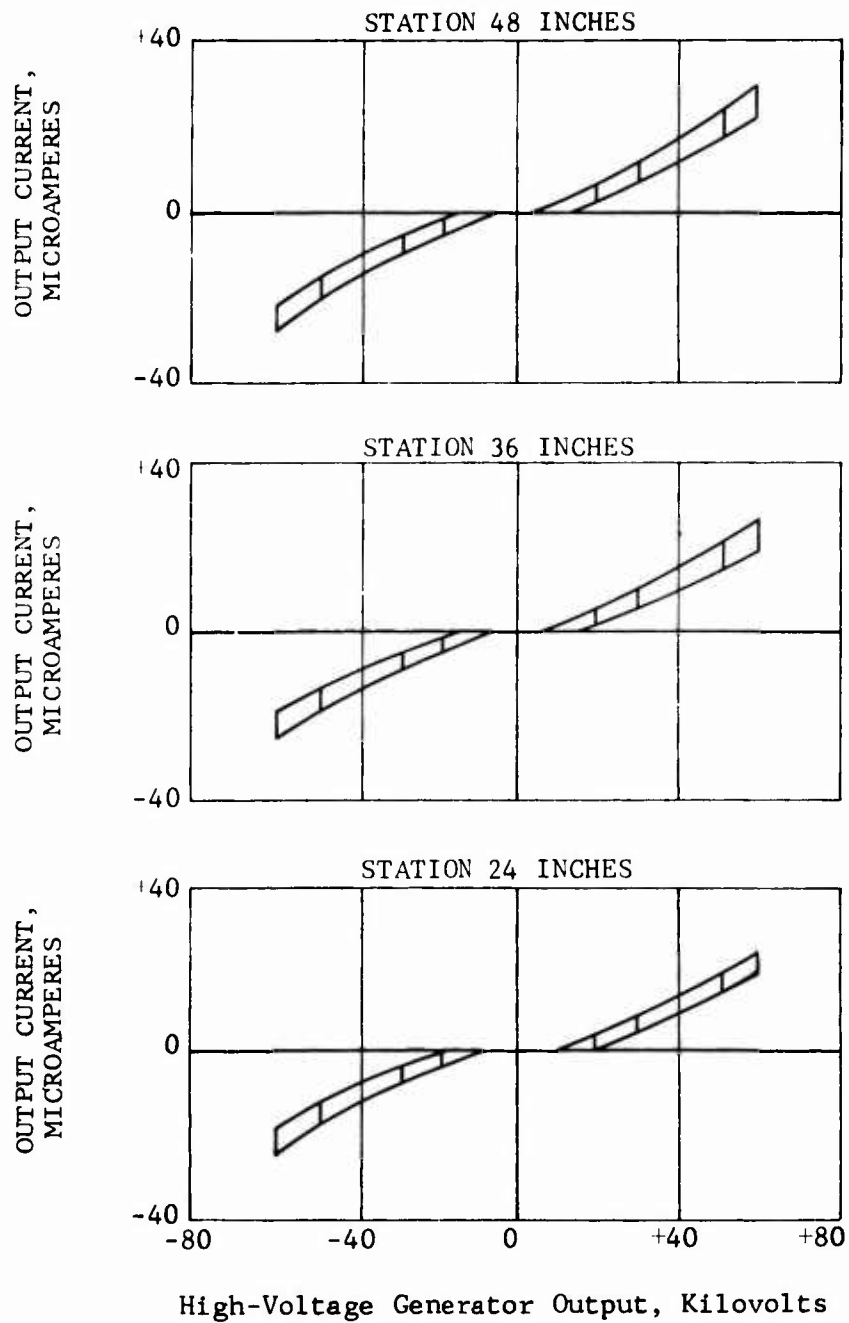


FIGURE 27: ENGINE-EXHAUST-MOUNTED CORONA POINT PERFORMANCE, CH-37 AIRCRAFT

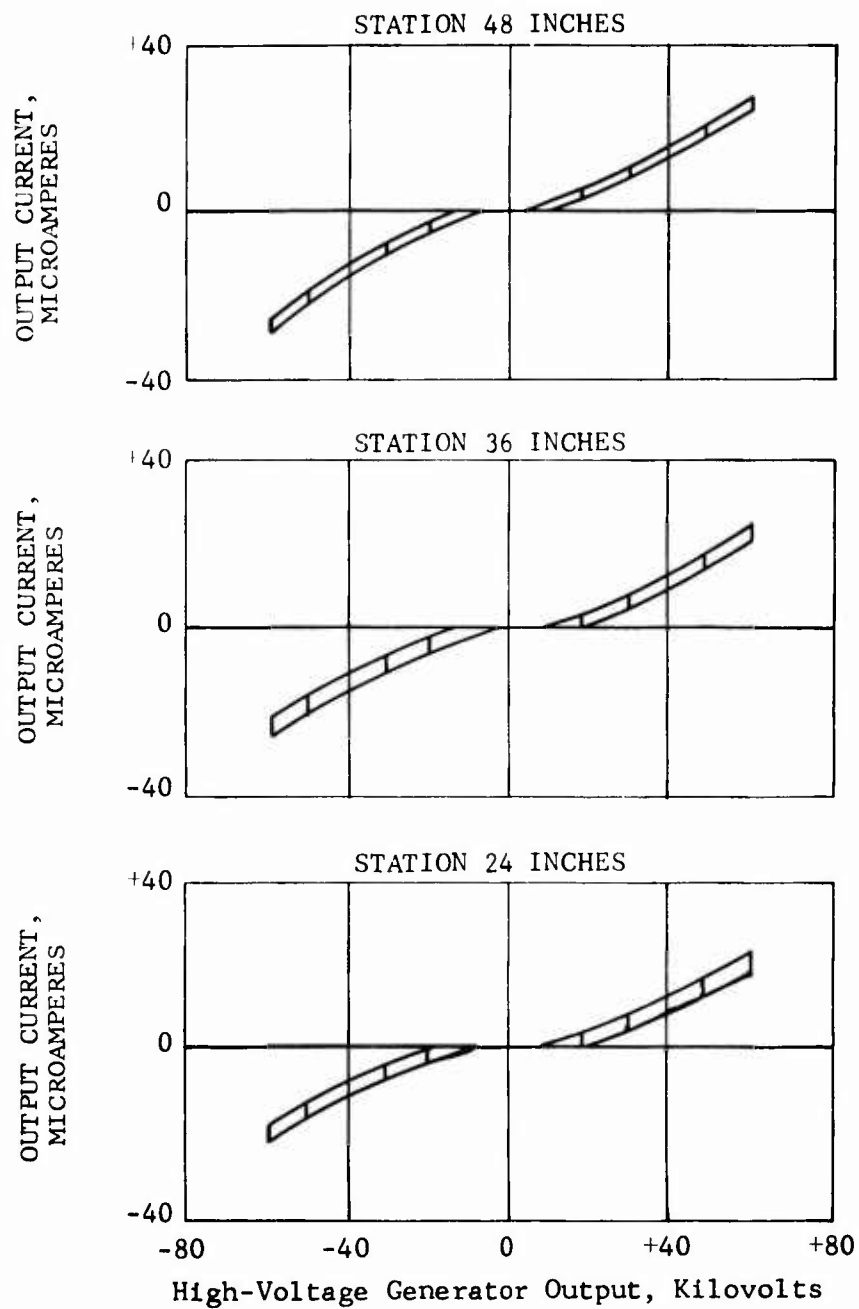
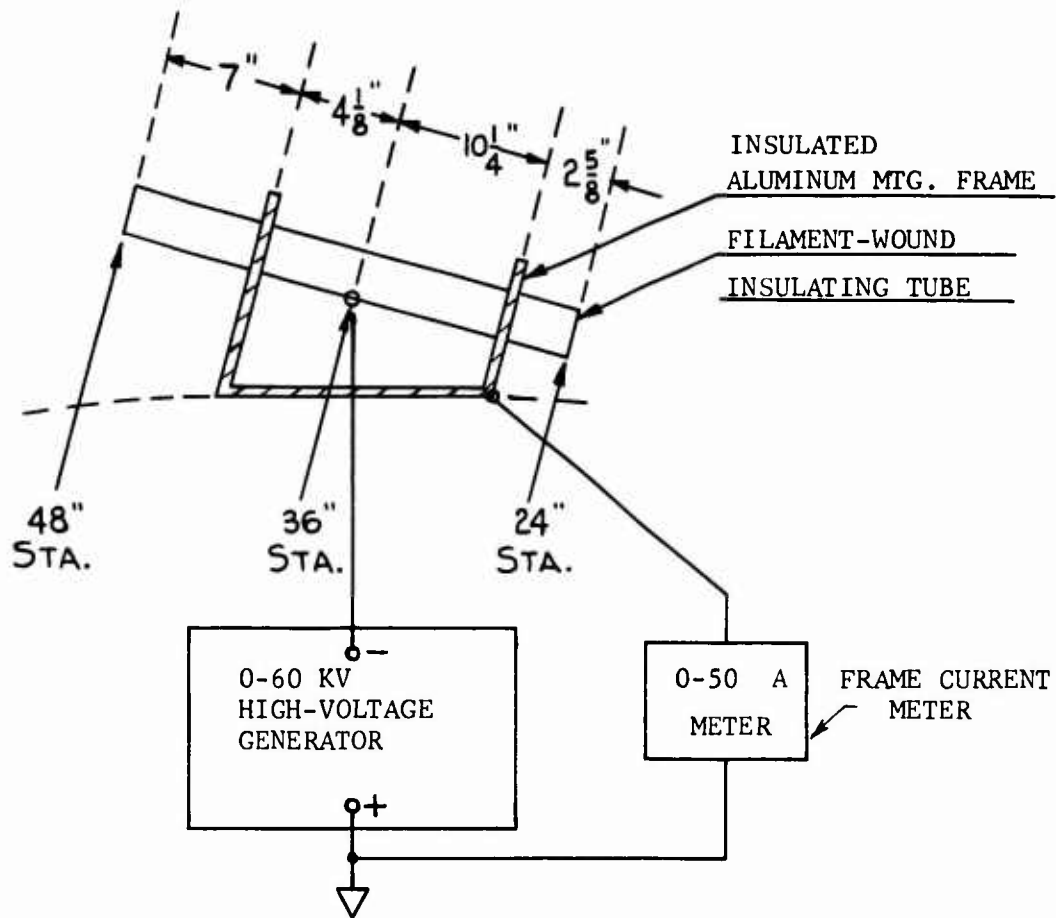


FIGURE 28: ENGINE-EXHAUST-MOUNTED CORONA POINT PERFORMANCE, CH-47A AIRCRAFT



Voltage, Kilovolts	Frame Current, Microamperes		
	STATION		
	48"	36"	24"
0	0	0	0
20	12	15	20
30	19	20	26
40	24	30	Arcover
50	30	Arcover	Arcover
60	Arcover	Arcover	Arcover

FIGURE 29: PROBE MOUNT LOSS TEST SET UP

2. Type 1 Discharger Performance

The Type 1 electrostatic discharging system was installed in a CH-37 helicopter and flight tested at Fort Rucker, Alabama.

Three types of tests were conducted in this phase of the test program:

- a. System transient response
- b. System operation during a typical CH-37 flight mission
- c. Touch tests

The system transient response tests were performed as follows: With the hovering aircraft short-circuited to ground through the dropline, the sensing unit of the discharging system was turned on while the power switch of the system remained "off". For this condition, the sensor output was recorded on Channel 1. Obviously, with the power switch in the "off" position, the discharging system was inoperative. Then, the continuity between the ground and the aircraft was broken in one of the high-voltage connectors in series with the ground line. The plug was not completely removed from its socket. In this manner, an air gap of a length varying between 3/8 inch and 3/4 inch was present in the partially open high-voltage connector.

As soon as the continuity between the aircraft and ground was lost, the aircraft potential began to rise under the action of the natural charging current. This rise was observed on Channel 2 of the recorder. After a certain period of time, the aircraft-to-ground voltage exceeded the dielectric strength of the air gap in the high-voltage connector, producing a discharging spark through which the aircraft was discharged to a low potential level. This spark discharge was clearly identifiable on the records, and its rate of repetition was also determined after a small number of consecutive discharges were observed.

The potential of the aircraft at the moment of the spark discharge was obviously well over the potential of saturation of the sensing unit of the electrostatic discharger and its associated recording channel. However, the magnitude of this

potential was approximately determined by the length of the spark gap, and was correlated with sparks of the same length obtained in the same connector by using a metered high-voltage power supply. Breakdown voltages ranging from 25,000 to 50,000 volts were obtained in this manner.

It should be pointed out that the actual magnitude of the aircraft voltage at or near the gap breakdown was of no significance for the purpose of the test. The only condition required for the experiment consisted of insuring that the aircraft potential was well above the sensor saturation level at the moment of the subsequent action. This action consisted of turning on the system power switch at the time of high aircraft voltage in order to analyze the behavior of the discharger during the subsequent period. Records obtained in this manner are reproduced in Figures 30 through 34.

System operation tests during a typical CH-37 flight mission were performed by flying the helicopter in a representative flight pattern while the system was in operation. The flight mission included taxiing, taking off, hovering, and landing. Figure 35 reproduces selected portions of the records during several parts of the cross-country flight.

Finally, the touch tests were performed by test personnel standing on the ground and physically touching a steel cable hanging from the hovering aircraft and electrically connected to the air frame. Both contractor personnel and U. S. Army enlisted men participated in the touch tests. No electrical sensations of any kind were experienced by these personnel.

3. Type 2 Discharger Performance

The Type 2 discharging system was tested in Phase 9 of the program, which was conducted at Fort Greely, Alaska.

At this test site (and its vicinity), previous natural charging readings (Reference 6) indicated natural charging currents of 50 microamperes in a CH-37 aircraft. This high natural charging current condition was the basis of the system performance specifications and of the selection of Fort Greely as a test site for the present research program. During this part of the test program, values of natural charging current exceeding 50 microamperes were measured.

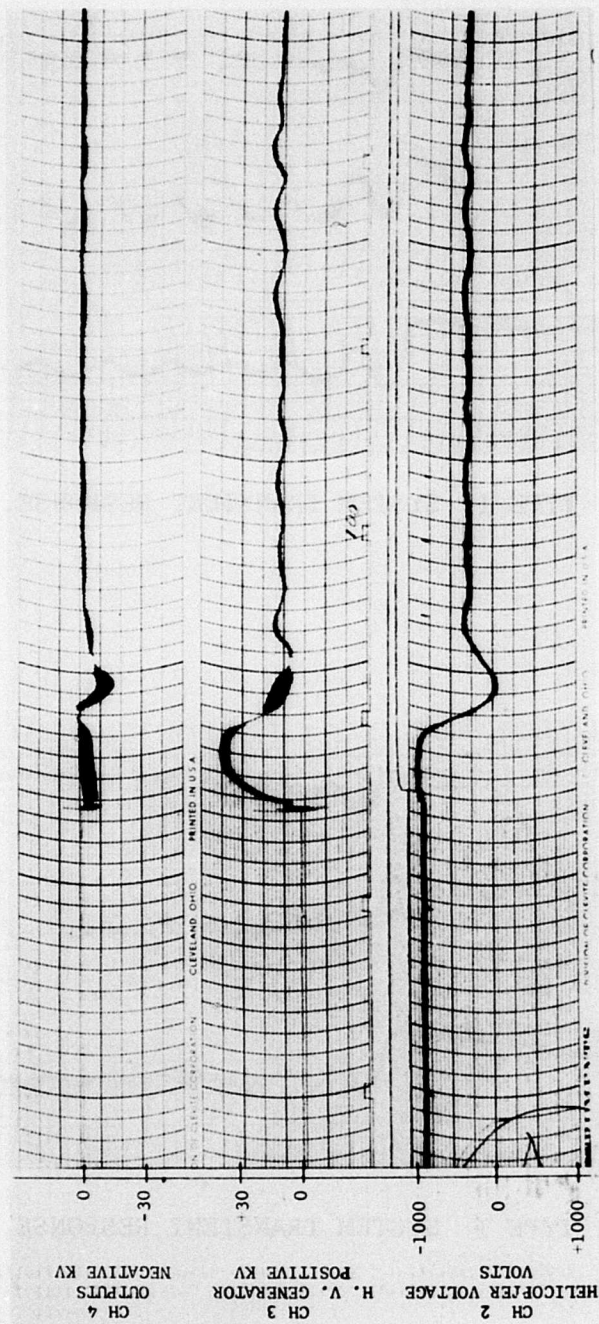


FIGURE 30: TYPE 1 SYSTEM TRANSIENT RESPONSE, GAIN 1

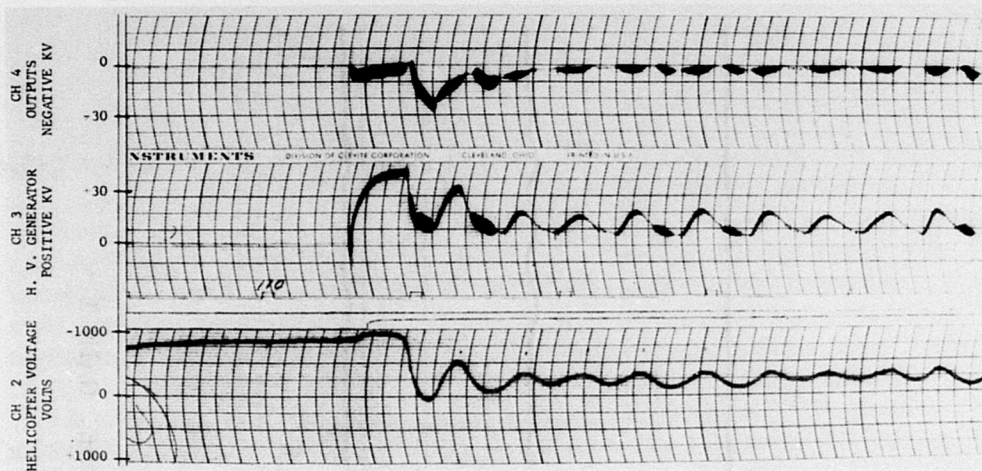


FIGURE 31: TYPE 1 SYSTEM TRANSIENT RESPONSE, GAIN 2

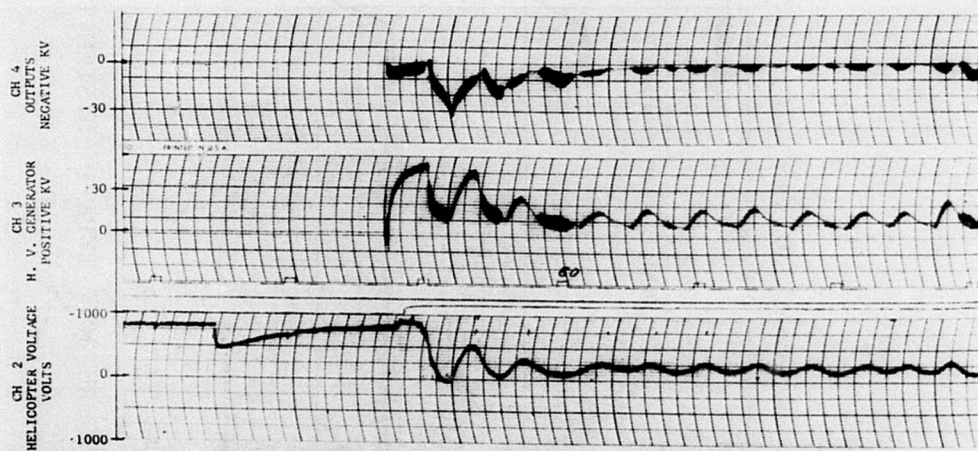


FIGURE 32: TYPE 1 SYSTEM TRANSIENT RESPONSE, GAIN 3

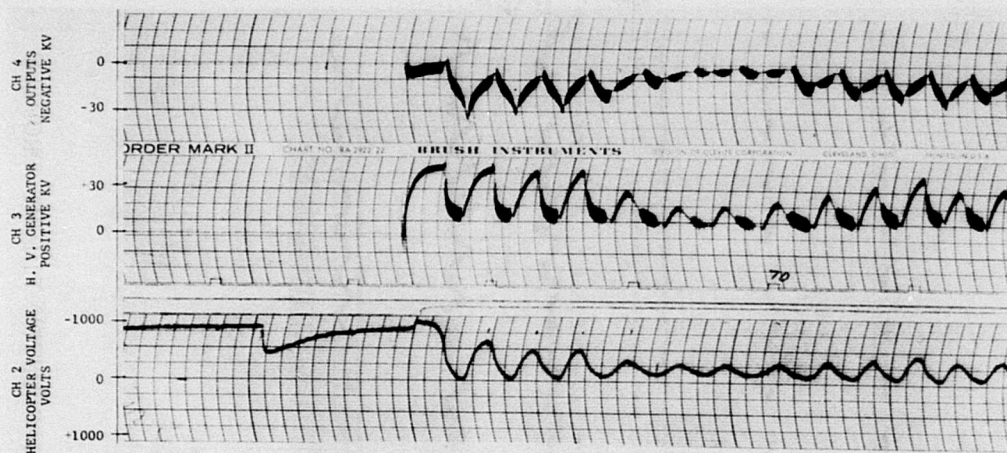


FIGURE 33: TYPE 1 SYSTEM TRANSIENT RESPONSE, GAIN 4

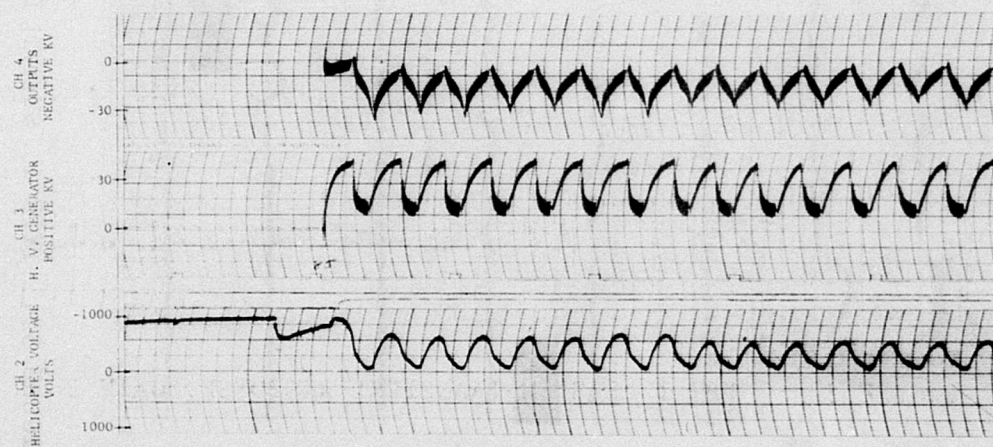


FIGURE 34: TYPE 1 SYSTEM TRANSIENT RESPONSE, GAIN 5

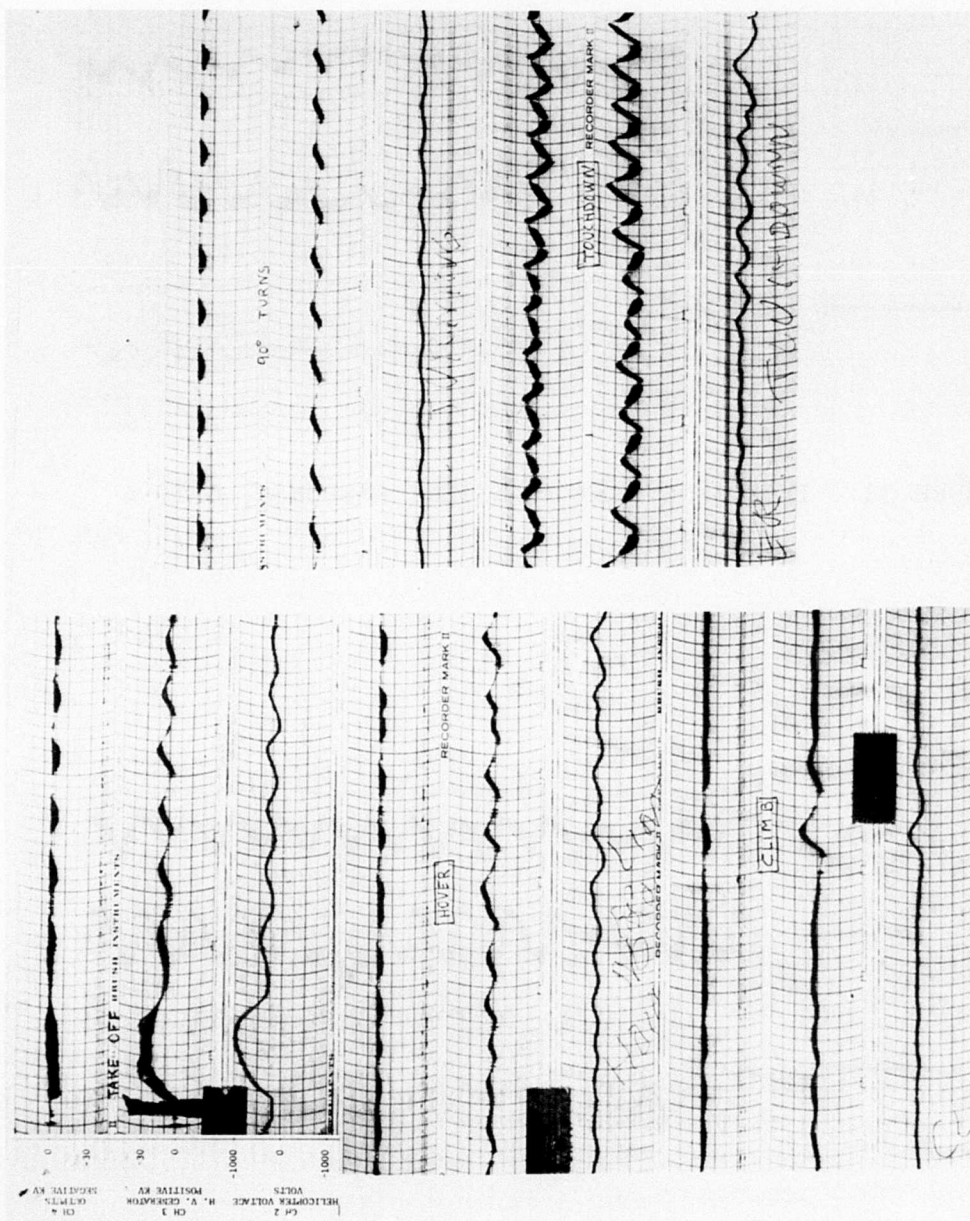


FIGURE 35: TYPE 1 SYSTEM PERFORMANCE IN CROSS-COUNTRY FLIGHT PROFILE

Occasionally, values as high as 120 microamperes were measured during a flight profile which was flown to create such high natural charges. This flight profile consisted of an approach to an area covered with snow, followed by hovering at a very low altitude at this site. Snow and ice crystals picked up by the rotor downwash were present during the hovering phase of this maneuver. Currents were recorded on Channel 1. Figure 36 shows a number of natural charging current records obtained during this type of flight. It may be seen that currents of up to 120 microamperes were recorded in one instance.

The visibility around the aircraft during the high charging periods was indeed very low. However, the pilots of the aircraft were still capable of obtaining ground references for their hovering flight. In fact, the pilots reported that still denser clouds are sometimes formed around helicopters engaged in arctic operations. These clouds may remain for a period of time, the length of which is dependent on the depth of the loose ice and snow cover on the ground.

The presence of these larger natural charging currents made it possible to test the discharging system under saturated conditions. This was done by repeating the flight profile described above with the discharging system in operation. Figures 37 and 38 are oscillograph traces obtained during these tests. It can be seen that both positive and negative system saturation conditions were recorded. The negative values were expected as a result of the relative position of ice crystals and aircraft surface material in the triboelectric series. On the other hand, the presence of high positive charging rates is not well understood at the present time. However, it was clearly recorded in some of the tests, as illustrated in Figure 38.

In addition to the saturation tests, this phase of the program included transient tests performed as described previously in Section D 2. Records obtained during these tests are reproduced in Figures 39 through 41.

Cross-country flights in arctic environments were also undertaken with the system in operation. Figure 42 reproduces selected parts of the records so obtained.

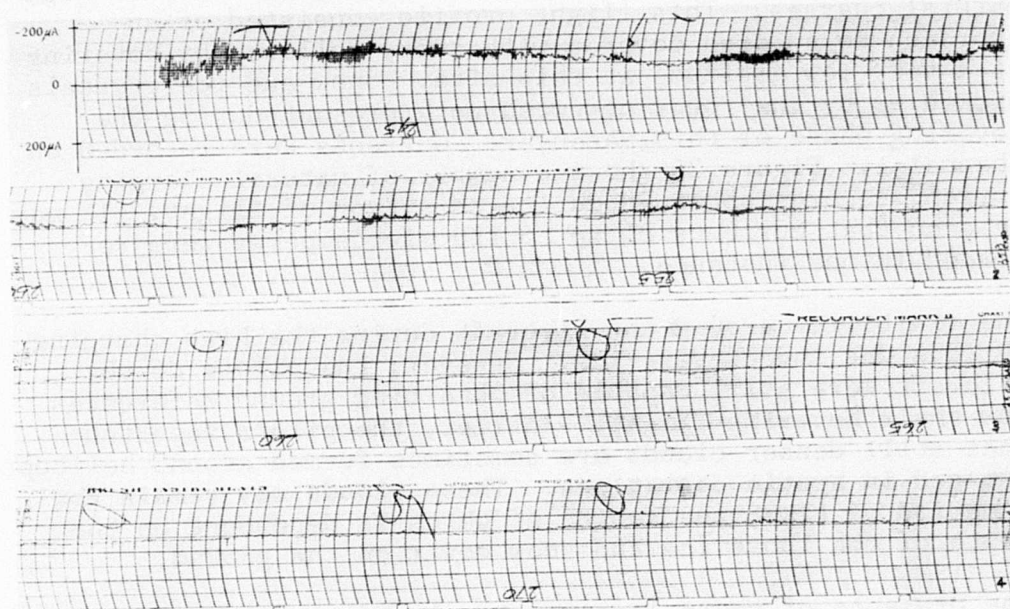


FIGURE 36: NATURAL CHARGING CURRENT RECORDS
(FORT GREELY, ALASKA)

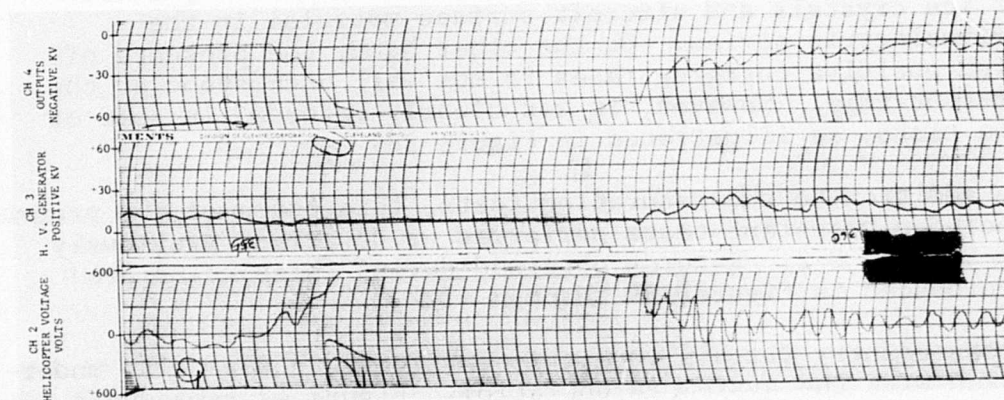


FIGURE 37: TYPE 2 DISCHARGING SYSTEM UNDER NEGATIVE
SATURATION CONDITIONS

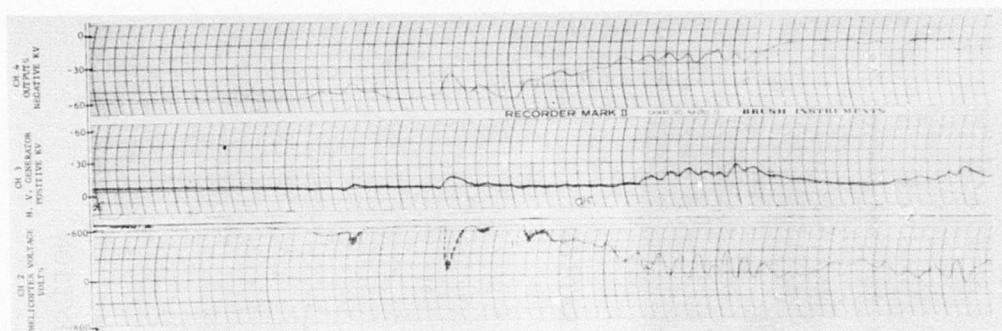


FIGURE 38: TYPE 2 DISCHARGING SYSTEM UNDER POSITIVE SATURATION CONDITIONS

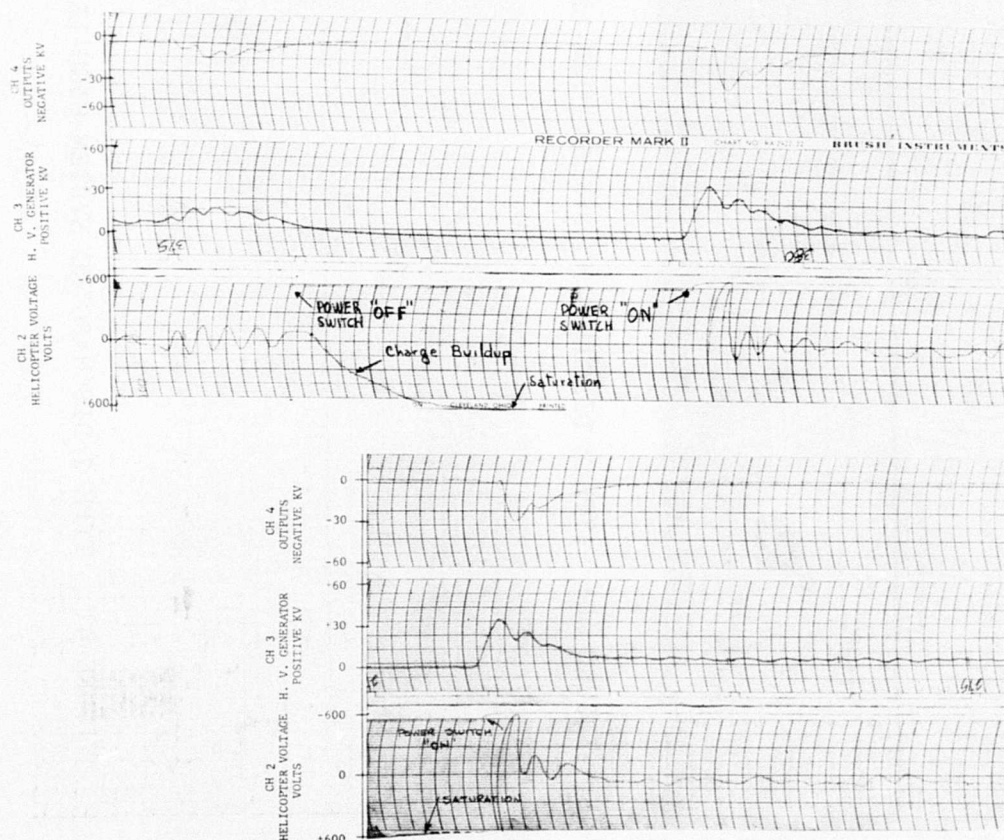


FIGURE 39: TYPE 2 DISCHARGING SYSTEM TRANSIENT RESPONSE

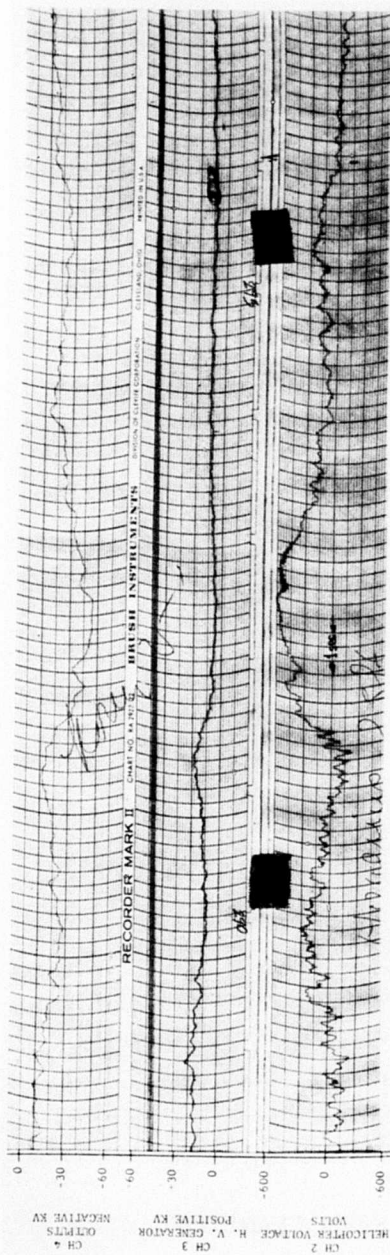


FIGURE 40: TYPE 2 DISCHARGING SYSTEM HIGH-LEVEL OPERATION

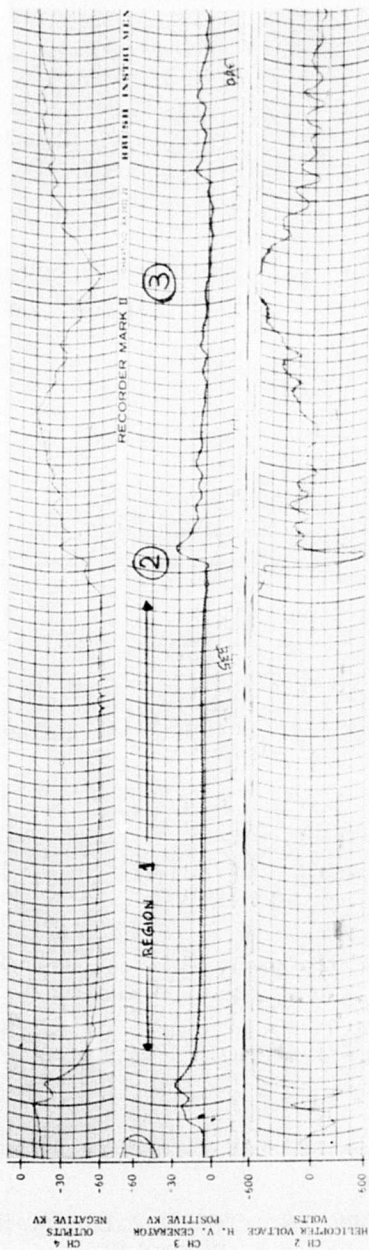


FIGURE 41: TYPE 2 DISCHARGING SYSTEM HIGH-LEVEL OPERATION

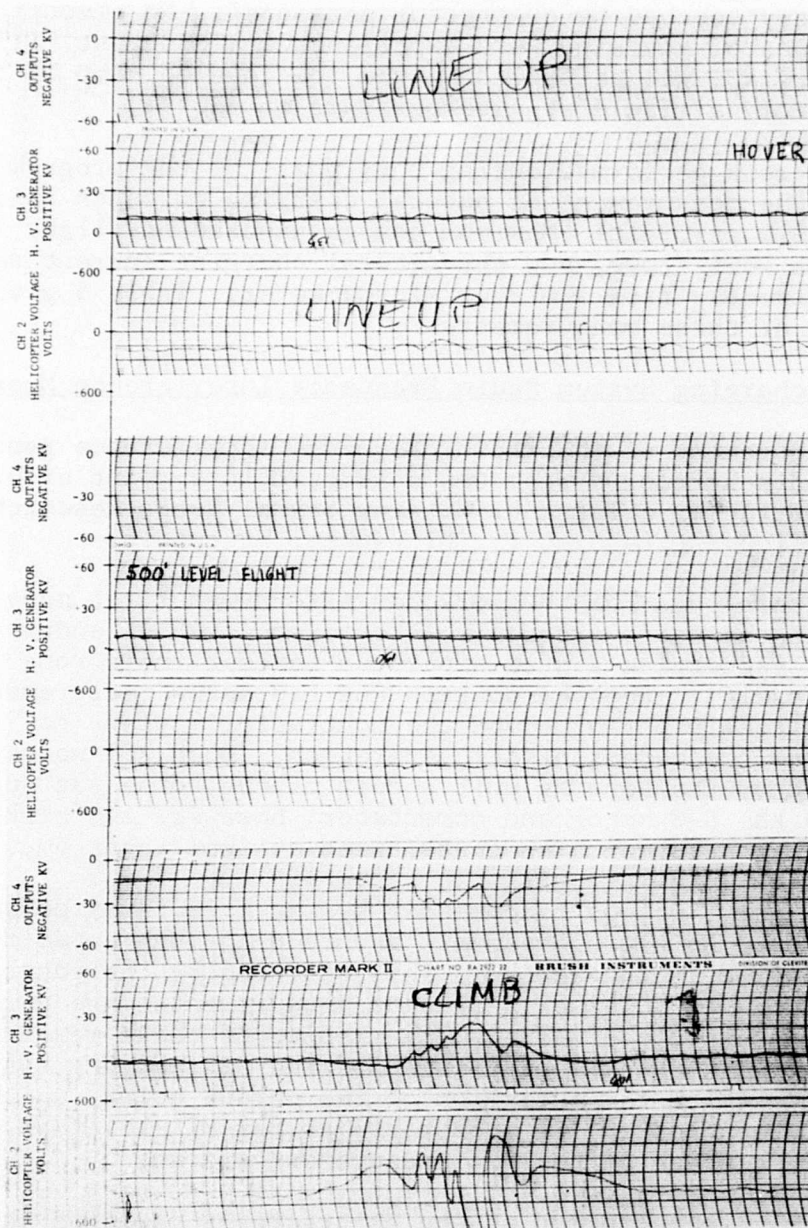


FIGURE 42: TYPE 2 DISCHARGING SYSTEM IN ARCTIC CROSS-COUNTRY FLIGHT PROFILE

Finally, a ground line hanging from the helicopter was repeatedly touched by contractor personnel. No electric sensations of any kind were experienced. This test, illustrated in Figure 43, was performed on the ice-covered ramp of the Fort Greely airfield at a temperature of -30°F .

Further work performed during this phase of the program included the measurement of natural charging currents in an Army UH-1D aircraft. Maximum charge-generating flight profiles were flown, and the natural charging current was taken directly from a mirror microammeter. Table 5 gives the results of these measurements.

4. Discharging System Radio Frequency Interference Measurements

The measurement of the radio frequency interference generated by the discharging system was conducted in a joint effort by this contractor and the U. S. Army Signal Corps Research and Development Laboratory, Milwaukee, Wisconsin.

During this phase of the work, an effort was first made to suppress the radio frequency interference (RFI) generated by the discharging system apparatus (except the corona point itself). Both conduction and radiation measurements were initially performed at the contractor's plant to determine the extent of RFI generation. Much RFI noise was produced by the sensing unit. Most of the noise was generated by the D-C motor and commutator; however, the high-voltage transformer also contributed a significant amount.

Consequently, it was recommended by the U. S. Army personnel that proper shielding elements and feed-through capacitors be installed in the system. This was done by the contractor, and subsequently, a new series of measurements were performed at the contractor's plant. The results of these measurements indicate that the RFI generation of the discharging system apparatus (with the exception of the corona point, which had not yet been tested) is acceptable as per MIL-I-11748B. Figure 44 shows a phase of the RFI measurement effort.

No tests were performed at the contractor's plant on the RFI produced by the high-voltage probes, due to the difficulty of the simulation of wind speed on the points. It was considered that the effect of wind on the space charge distribution would substantially affect the whole ion generating



FIGURE 43: TOUCH TESTS, FORT GREELY, ALASKA

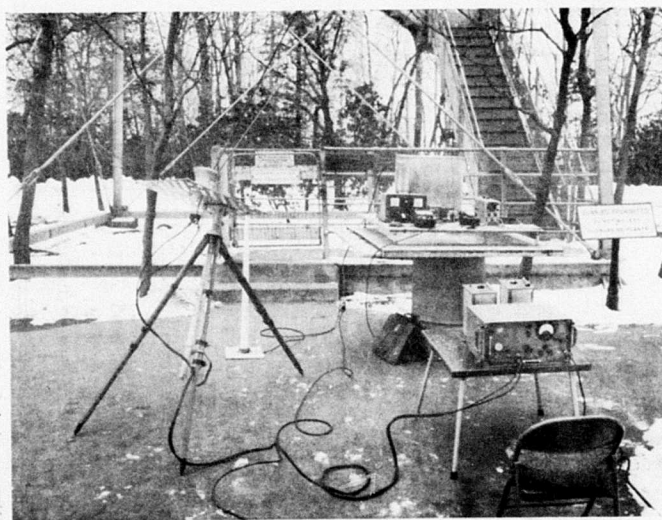


FIGURE 44: RADIO FREQUENCY INTERFERENCE MEASUREMENTS

600451

TABLE 5
UH-1 HELICOPTER NATURAL CHARGING CURRENT DATA.

ARCTIC ENVIRONMENT

Approach Point Characteristics	Natural Charging Current (Microamperes)		
	During Approach	Peak Value	5 feet Alt. Hovering
Iced River Bed	-2	-18	-4
Mountain Glacier	-3	-25	-5
Loose Snow on Ground	+3, -3	-35	-3
Crystallized Ice (Ramp)	-1	-10	-3
Snow-Covered Runway	+1, -1	-12	-4

process; consequently, this test should be performed under the same environmental conditions expected for the corona points in an actual installation. Consequently, the measurement of the RFI produced by the corona probes was conducted at Edwards Air Force Base, California, with the support of the U. S. Army Aviation Test Office, Edwards Air Force Base. Because of unforeseen problems which could not be overcome in the time allocated for the tests, the test equipment had to be located on the ground instead of in the aircraft. With the antenna located on the ground, the RFI noise generated at the points was found to substantially exceed the maximum limits established by MIL-I-11748B. Two types of corona point probes were used, as shown in Figure 45. This figure is considered to be self-explanatory.

The results of the RFI measurements were reported by the U. S. Army Signal Corps Research and Development Laboratory. A copy of this report is included as Appendix B.

During this phase of the program, the natural charging current generated by a CH-37 aircraft in a sandy environment was also measured. The aircraft was flown in a vertical descent over an area in the Mojave Desert used for tank artillery tests. The frequent passage of tracked vehicles over this dry, sandy area developed a thick layer of loose, fine sand which enveloped the helicopter when blown by the rotor downwash as the altitude of the aircraft decreased from a 100-foot hovering altitude to a few feet above the ground. Natural charging current peaks of near 40 microamperes were recorded in this manner for short periods of a few seconds each by the use of a dropline connected to a wire mesh ground plane. Only a limited number of test flights were made due to an aircraft engine failure which ended one of the hovering periods and made the test aircraft unavailable for additional flight tests.

F. ANALYSIS OF EXPERIMENTAL RESULTS

1. Discharging System Performance

The Type 2 discharging system used in this program meets the design specifications of keeping the electrostatic energy of a CH-37 helicopter below 1 millijoule (1200 volts at 5 feet of altitude) for natural charging currents of up to 50 microamperes.

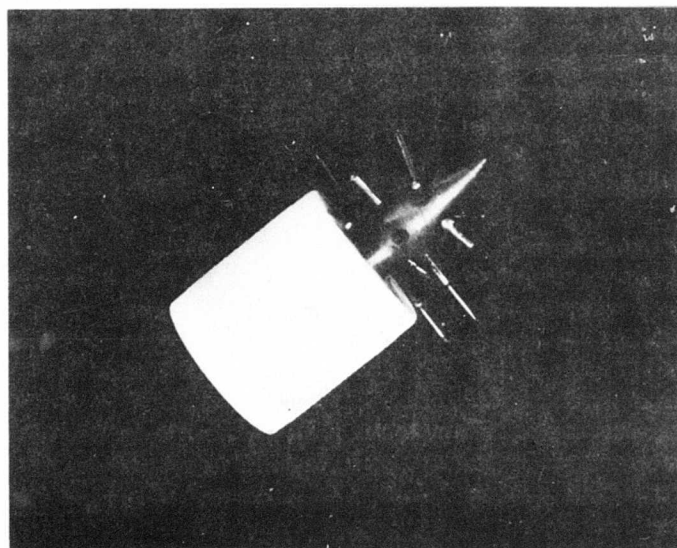


FIGURE 45: CORONA POINT PROBES USED IN THE RFI MEASUREMENTS

Based on an analysis of the flight test data, it is believed that the Type 2 discharging system tested in this program is adequate for most operational conditions. Examples of flight test records illustrating the performance and the dynamic stability of this discharging system are presented in Figures 39, 40, and 41. The good dynamic stability of the system is shown in Figure 39. The rapid decay of the helicopter voltage illustrates the adequate damping of the system. Figure 40 shows the system performance during a relatively high charging rate. The negative high-voltage generator shows a maximum output of 46 KV, which is equivalent to a discharging rate of about 38 microamperes. It is noted that the helicopter voltage is kept below 600 volts. A maximum performance test is illustrated in Figure 41. In Region 1 of this figure, the system was saturated. The negative high-voltage generator is operating at 60 KV (equivalent to a 50-microampere discharging current), while the helicopter voltage exceeds the 600-volt saturation limit (due to natural charging currents in excess of 50 microamperes). At Point 2 on Figure 41, the system becomes unsaturated and the helicopter voltage is reduced to acceptable levels. The system performance limits are clearly indicated at Point 3, where the negative high-voltage generator operates at close to 60 KV (equivalent to about 50 microamperes discharging current, which in steady state is equivalent to the charging rate); the helicopter voltage is at 600 volts, which is still 600 volts below the specified maximum permissible value for the CH-37 helicopter at the test altitude of 5 feet.

2. Correlation of Theory and Experimental Data

An important result of the analysis of the experimental data was the good correlation of these data with the theoretical prediction of the system performance. As mentioned previously, this program utilized both theory and experimental data to arrive at the design values of the Type 2 discharger. The first test series utilized the Type 1 discharger. This discharger possessed an invariable value of the time constant ($T_g = 0.3$ second), which for the design gain ($K_{c1} = 8 \times 10^{-3}$) is equivalent to a damping ratio of $\zeta = 0.125$. In order to obtain test data for other damping ratios, provisions were made for varying the system gain.

The test values of the system gain were determined by means

of theory. The good correlation between theory and Type 1 discharger experimental data is demonstrated by comparing the test data shown in Figures 30 through 34 with the computer traces of Figure 19. These test data and the analytical curves shown in Figure 18 were utilized to determine the time constant for the dynamic compensator, T_c , used in the Type 2 discharger.

The improved stability that was obtained by use of the dynamic compensator is shown in Figure 46, which presents test data on the response to a disturbance of the system with and without the dynamic compensator (Type 2 and Type 1 dischargers, respectively).

It should be noted here that because of the lack of an existing theory, the transfer functions of the sensor and the corona points were obtained using empirical data. Additional theoretical work should be performed to obtain a better understanding as well as to possibly provide improved performance of these system components.

3. Natural Charging Currents

A maximum natural charging current of 50 microamperes was specified for the discharging system used in this program. This value was based on earlier measurements performed by the U. S. Army. However, during the present program, flight maneuvers were performed with the intent of exceeding these previously obtained values. These maneuvers consisted, for example, of a low-altitude flare-out over an area covered with snow. Test data obtained during these maneuvers indeed indicated the existence, over periods of several seconds, of charging currents in excess of 50 microamperes. Maximum values of about 120 microamperes were obtained in the arctic, as shown in Figure 36. In the desert, values of 40 microamperes were recorded. However, the influence of these high-charging maneuvers on the establishment of practical discharger design criteria should be evaluated. This can best be accomplished by installing Type 2 dischargers together with slow-speed recorders in a number of operational helicopters. This will obviate the use of ground lines to measure charging current; hence, it will permit normal helicopter operation and also will provide an adequate statistical sample of charging data for various missions and weather conditions.

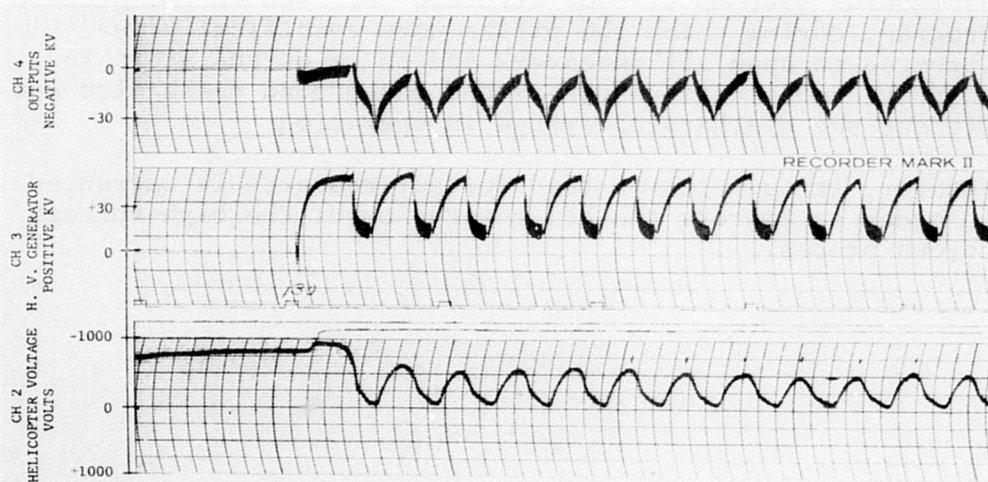
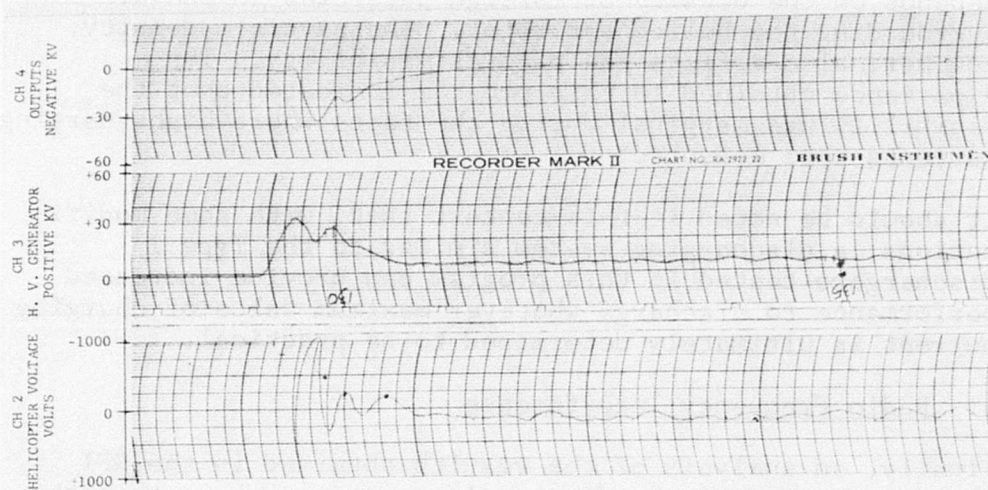


FIGURE 46: COMPARISON OF SYSTEM RESPONSE TO A TRANSIENT WITHOUT (TYPE 1) AND WITH (TYPE 2) DYNAMIC COMPENSATION

It is believed that in any case there exist other factors which would limit the maximum discharger requirements. For example, the magnitude of the natural charging current depends on the density of foreign particles in the air surrounding the helicopter rotor. The particle density, however, also affects the pilot's visibility. The experience obtained in this program indicated that the visibility was marginal during the tests where high charging currents were measured.

It should be noted in this context that, with some modifications, a discharging system similar to the Type 2 dischargers tested in this program can provide increased performance to discharge whatever maximum value of charging current is ultimately determined to be practical.

4. Radio Frequency Interference

Finally, an analysis of the results obtained in the RFI characteristics of the discharging system reveals that the high-voltage probes are the only RFI problem area yet to be fully understood. It must be mentioned, however, that no interference was detected in any of the communication or navigation systems of four aircraft utilized in the present program, during which the pilots were specifically instructed to open all receivers and to be on the alert for any noticeable differences in the background noise with and without the discharging system in operation.

However, it is believed that further research is warranted in order to improve the RFI generation of the high-voltage corona probes.

BIBLIOGRAPHY

1. de la Cierva, J., "Helicopter Static Electricity Discharging Device," TCREC Technical Report 62-33, U. S. Army Transportation Research Command, Fort Eustis, Virginia, December, 1962.
2. de la Cierva, J., "Evaluation of a Helicopter-Fuselage-Mounted Dynamic-Neutralizer Static Electricity Discharging System," TCREC Technical Report 62-93, U. S. Army Transportation Research Command, Fort Eustis, Virginia, December, 1962.
3. Stimmel, R. G., et al, "Army-Navy Precipitation Static Project," Volume 34, Nos. 4 and 5, Proceedings Institute of Radio Engineers, April and May 1946.
4. "Study and Investigation of Methods of Dissipation of Static Electricity on Helicopters," TREC Technical Report 60-55, U. S. Army Transportation Research Command, Fort Eustis, Virginia, September, 1960.
5. Tona, C. J., "Automatic Control of Static Electricity for Army Helicopters," TREC Technical Report 61-18, Phase I Report, U. S. Army Transportation Research Command, Fort Eustis, Virginia, February, 1961.
6. Seibert, J. M., "Helicopter Static - Electricity Measurements," TREC Technical Report 62-72, U. S. Army Transportation Research Command, Fort Eustis, Virginia, June, 1962.

APPENDIX A

ANALOGUE COMPUTER ANALYSIS

An analogue computer analysis of the discharger system dynamics was performed. The system equations are as follows:

$$I_t = I_n - I_d \quad (A-1)$$

$$V_H = \frac{I_t}{C_H s} \quad (A-2)$$

$$V_s = K_s V_H \quad (A-3)$$

$$V_c = K_{c1} V_s \quad (A-4)$$

$$V_a = K_a V_c \quad (A-5)$$

$$V_{cp} = \frac{K_g}{1 + T_g s} V_a \quad (A-6)$$

$$I_d = K_{cp} V_{cp} \quad (A-7)$$

The symbols are defined in the block diagram shown in Figure 15. The symbol s is the Laplace operator. Values for the system constants are as follows:

$$C_H = 10^{-9} \text{ farads}$$

$$K_s = 3 \times 10^{-3} \frac{\text{VOLTS PEAK}}{\text{VOLTS DC}}$$

$$K_{c1} = \begin{array}{l} \text{to be varied between } 2.67 \times 10^{-3} \\ \text{and} \\ 13.31 \times 10^{-3} \frac{\text{VOLTS PEAK}}{\text{VOLTS PEAK}} \end{array}$$

$$K_a = 10^3 \frac{\text{VOLTS PEAK}}{\text{VOLTS PEAK}}$$

$$K_g = 2.5 \times 10^3 \frac{\text{VOLTS DC}}{\text{VOLTS PEAK}}$$

$$T_g \text{ to be varied between } 0.03 \text{ and } 0.5 \text{ second}$$

$$K_{cp} = 0.835 \times 10^{-9} \frac{\text{AMPERES DC}}{\text{VOLTS DC}}$$

The machine equations used in the computer are:

$$\left(\frac{I_t}{5 \times 10^{-5}} \right) = \left(\frac{I_n}{5 \times 10^{-5}} \right) - \left(\frac{I_d}{5 \times 10^{-5}} \right) \quad (\text{A-8})$$

$$\left(\frac{V_H}{2000} \right) = \frac{25}{s} \left(\frac{I_t}{5 \times 10^{-5}} \right) \quad (\text{A-9})$$

$$\left(\frac{V_s}{10} \right) = 0.6 \left(\frac{V_H}{2000} \right) \quad (\text{A-10})$$

$$\left(\frac{V_c}{0.05} \right) = 0.2 \left(10^3 K_{c1} \right) \left(\frac{V_s}{10} \right) \quad (\text{A-11})$$

$$\left(\frac{V_a}{50} \right) = \left(\frac{V_c}{0.05} \right) \quad (\text{A-12})$$

$$\left(\frac{V_{cp}}{6 \times 10^4} \right) = \frac{2.09}{1 + T_g s} \left(\frac{V_a}{50} \right) \quad (\text{A-13})$$

$$\left(\frac{I_d}{5 \times 10^{-5}} \right) = \left(\frac{V_{cp}}{6 \times 10^4} \right) \quad (\text{A-14})$$

The analogue computer diagram of Equations (A-8) through (A-14) is presented in Figure 17. The helicopter voltage response ($V_H/2000$) was obtained to step inputs of the natural charging current ($I_n/5 \times 10^{-5}$). Both of these quantities were recorded as shown in Figure 17. Some of the computer records are shown in Figures 18 and 19. A discussion of these traces is presented in Section C 7.

APPENDIX "B"

C O P Y

U. S. ARMY ELECTRONICS RESEARCH & DEVELOPMENT LABORATORY

ADDRESS REPLY TO:
COMMANDING OFFICER
USAEIRD L FIELD STATION NO. 1
P.O. BOX 6262
MILWAUKEE 9, WISCONSIN

FIELD STATION NO. 1

6081 NORTH HOPKINS STREET
MILWAUKEE 9, WISCONSIN

SELRA/TS

26 April 1963

SUBJECT: Electrostatic Discharger for Helicopters, Contract DA-44-177-AMC-3(T), Dynasciences Corporation

TO: Commanding General
U. S. Army Transportation Engineering Command
Attention: SMOFE-ASE (Mr. S. B. Poteate)
Fort Eustis, Virginia

1. Reference our letter 5 June 1962, subject: "Project 9R38-01-017-30, Static Electricity Dissipator, Contract DA-44-177-TC-843, Kellett Aircraft Corporation."

2. Arrangements for further investigation of the subject unit to determine conformance to MIL-I-11748B were completed by Mr. Poteate of your office.

3. Tests were initiated at the contractor's plant, Fort Washington, Pennsylvania, to develop a satisfactory suppression system for the various components of the discharger. This was accomplished using standard suppression techniques. No attempts were made at that time to evaluate the interference from the corona points although interference was noted from the corona points from 1.8 mc to 40.0 mc.

4. Tests were conducted at Edwards AFB with the intent of evaluating the interference from the corona points with the aircraft in flight. The radio interference reduction equipment was set up on the flight strip in line with the corona points on the aircraft. Tests with the aircraft hovering were conducted at various distances with both wick type and needle type corona discharge points. At the greatest distance tested, 18 feet, the electrical discharge from the corona points exceeded the permissible limits over the frequency range of 8 to 40 mc. From these tests it is evident that the corona points can produce high levels of interference. However, the determination was made with the antenna located on the ground while the aircraft

C O P Y

C O P Y

SELRA/FS

26 April 1963

SUBJECT: Electrostatic Discharger for Helicopters, Contract DA-44-177-AMC-3(T), Dynasciences Corporation

hovered, which could introduce interference because of the corona field using the antenna as a path to ground. Originally the plan was to test the discharger with the test equipment located in the aircraft, however this was not possible because of many unforeseen problems which could not be overcome in the time allocated for the test.

5. It can be concluded that a radio interference reduction system can be designed for the discharger components developed by Dynasciences using standard suppression techniques. However, the corona points will need further evaluation before a definite conclusion and analysis can be made for the corona while the aircraft is in flight.

6. It is recommended that further studies be carried out to evaluate the corona with respect to RF generation. It is further recommended this evaluation be carried out by a private testing laboratory because the current heavy workload and manpower shortage will not allow this Station further work in this area. This Station will be pleased to furnish any further information you may require or attend any meetings to discuss this matter in greater detail.

G. C. HOWARD
Captain, SigC
Commanding

Copy furnished:

Dynasciences Corp.
Attn: Mr. Juan DeLaCierva
Ft Washington Industrial Park
P.O. Box 351
Fort Washington, Pennsylvania

CO, USAELRDL
Attn: SELRA/GF
Ft Monmouth, NJ

C O P Y